National Library of Canada

Acquisitions and Bibliographic Services Branch

395 Wellington Street
Ottawa, Ontario
K1A 0N4

Bibliothèque nationale du Canada

Direction des acquisitions et des services bibliographiques

395, rue Wellington
Ottawa (Ontario)
K1A 0N4

Your file Votre référence

Our file Notre référence

NOTICE

The quality of this microform is heavily dependent upon the quality of the original thesis submitted for microfilming. Every effort has been made to ensure the highest quality of reproduction possible.

If pages are missing, contact the university which granted the degree.

Some pages may have indistinct print especially if the original pages were typed with a poor typewriter ribbon or if the university sent us an inferior photocopy.

Reproduction in full or in part of this microform is governed by the Canadian Copyright Act, R.S.C. 1970, c. C-30, and subsequent amendments.

AVIS

La qualité de cette microforme dépend grandement de la qualité de la thèse soumise au microfilmage. Nous avons tout fait pour assurer une qualité supérieure de reproduction.

S'il manque des pages, veuillez communiquer avec l'université qui a conféré le grade.

La qualité d'impression de certaines pages peut laisser à désirer, surtout si les pages originales ont été dactylographiées à l'aide d'un ruban usé ou si l'université nous a fait parvenir une photocopie de qualité inférieure.

La reproduction, même partielle, de cette microforme est soumise à la Loi canadienne sur le droit d'auteur, SRC 1970, c. C-30, et ses amendements subséquents.

Canada

Single Crystal Surface Investigations Using RHEED

by

John Bulicz

Thesis submitted to the School of Graduate Studies and Research in partial fulfillment of the requirements for the degree of Master of Science in Physics

Physics Department
Faculty of Science
University of Ottawa
Ottawa, Canada

ISBN 0-315-85820-6

Canada

UNIVERSITÉ D'OTTAWA
UNIVERSITY OF OTTAWA

Abstract

A RHEED system was assembled and incorporated in the existing ultra-high-vacuum chamber. A system for the production and transport of low energy ions to the ultra-high-vacuum environment was maintained. Samples cut from wafers of Si(100) were investigated using electron diffraction as well as low energy ion scattering techniques. The surface composition, symmetry and orientation of these specimens could be determined. Attempts to adsorb hydrogen onto the Si(100) surface indicated that the procedure in use needs to be modified. An initial RHEED study of the Si(110) surface revealed a complex arrangement of atoms which does not correspond to the "16x2" structure reported for the clean surface.

Acknowledgements

I would like to express my deep appreciation to Dr. Brian Hird for inviting me to join in the development of the facilities for surface studies, an opportunity to work in an environment conducive to the development of practical skills and methods associated with experimental research and for providing encouragement and guidance throughout my association with the project.

I am grateful to have had the opportunity of working in the company of Dr. Robert Armstrong, from whose experience and insight I was able to benefit greatly.

I would like to thank Dr. Peter Piercy for his generosity in times of need.

The success of this enterprise owes much to the help and cooperation of Pierre Gauthier.

Many thanks to Bob Hart, Ron, Herve, Francois and, in particular, to Len Pement for the excellent machining, and generosity with both tools and advice. Thanks also go to Art Buser and Mike Murphy for their willingness to assist in all matters of an electronic nature.

Finally, I would like to thank my parents for the patience, tolerance, understanding and support they have shown during the period of this work.

Contents

List of Figures

Chapter 1. Introduction

The structure and composition of solid surfaces can be related to the mechanical, electronic and chemical properties exhibited by the material at the surface. This has motivated the development of several techniques for the study of the structural properties of crystal surfaces.

A necessary condition for successful investigation of crystal surfaces is the ability to maintain the surface free from undesired contamination for the duration of the experiment. The development in the 1950's of techniques for the achievement and maintenance of ultra-high-vacuum, a region below 10^{-9} torr, was an important factor in the growth of surface physics. Previous results were relatively meaningless because of surface contaminants. A monolayer of foreign atoms at the surface would substantially affect the measurements we proposed to take of a clean surface. At pressures in the 10^{-8} torr range, the surface becomes covered by a monolayer of Nitrogen in 5 minutes. Our base pressure of 2×10^{-10} torr provided a stable environment in which to carry out surface measurements.

Chapter 1. Introduction

The goal of this research was to build an apparatus and develop techniques for studying the symmetry, structure and composition of single crystal semiconductor surfaces using low energy ion scattering (LEIS) and reflection high energy electron diffraction (RHEED) under ultra high vacuum conditions. An apparatus that provided ion beam production and transport to the UHV chamber was maintained, and a RHEED system was assembled and incorporated in the UHV chamber.

RHEED is a common method used to investigate single crystal surfaces. Diffraction patterns caused by the interaction between X-rays and crystals are well known phenomena and yield information about bulk crystal symmetries. Electrons have a much lower penetration depth than X-rays and can be used to investigate the surface structure of a crystal. RHEED is a technique in which forward scattered electrons produce a diffraction pattern. The diffraction pattern from a clean sample will yield information about the structure of the surface. It has been used widely as a convenient method to determine crystal orientation. RHEED also provides an effective method of identifying structures formed by surface reconstruction or by the adsorpton of foreign atoms or molecules.

Since the work of Smith in the late 1960's[1] the scattering of low energy ions has been accepted as a useful technique for the

analysis of surface structures and the elemental composition of surfaces. Whereas RHEED images show large scale symmetries associated with the crystal, ion scattering experiments can be used to investigate interatomic relationsnips at the surface.

This thesis will give a description of the construction and operation of a RHEED system. The existing facilities for the production of low energy ion beams will be reviewed briefly, as the data available from ion scattering energy spectra provided additional information about the surface phenomena observed using RHEED. Furthermore, a description of the vacuum requirements for the system will be given since an ultra high vacuum environment is crucial in order to obtain meaningful results. Tests carried out using samples of Si(100) wafers will be described as well as a study of the Si(110) surface using only RHEED.

The RHEED system geometry was well suited to the space available in the UHV chamber. The qualitative information available from the RHEED images was used to determine not only the orientation of the surface, but also served as an aid in finding optimum settings for the electron beam heater. The great advantage of having an electron diffraction system available is that it provides immediate information about the state of the surface, whereas ion scattering measurements require a longer time to carry out. Thus RHEED is valuable as a diagnostic tool.

The Si(100) surface was chosen as a test sample as it has been studied extensively and a wealth of information about its structure and symmetry is readily available. Techniques associated with RHEED and LEIS as well as procedures for cleaning and heating the sample were refined in order to obtain results similar to well-established observations.

Ions detected following low energy oxygen ion collisions with the (100) surface of silicon provided information about ion scattering and recoil from the surface. This information determined the composition of the surface and was used to monitor the surface for indications of contamination.

The Si(110) surface has not been studied to the same degree as Si(100), however a number of electron diffraction studies have been carried out. Since information about this surface is scarce, a RHEED study was carried out to explore the low index crystallographic directions in the plane, and to observe the re-ordered surface structure following a heating procedure to clean the target.

The change in surface structure accompanying adsorption of Hydrogen atoms onto the Si(100) surface is a well-known phenomenon. A discussion of our procedure for dissociating H_2 molecules in the

UHV chamber and the resulting RHEED images will indicate certain modifications in our technique which will be required in order to successfully achieve the well known results obtained by others.

Chapter 2. Surface Physics Techniques

2.1 Reflection High Energy Electron Diffraction

The top few layers of crystals may be characterised using electron diffraction. The first experiment of Davisson and Germer[2] to verify the wave nature of electrons in 1927 was conducted using an apparatus which became the prototype for the modern Low Energy Electron Diffraction (LEED) system. Since the development of UHV facilities this technique has been extensively used as one of the primary methods to determine the structure of surfaces.

X-ray diffraction is the most common method for studying bulk structure. However, the penetration depth of x-rays is large making this technique insensitive to surface atoms. The penetration depth of neutrons is even larger and hence less sensitive to surface atoms. Electrons are approximately 1000 times more strongly scattered by atoms than are x-rays, making them a good candidate for surface studies.

The energy spectrum of a beam of monoenergetic electrons back-scattered from a solid surface is shown in figure 1. The large, broad maximum occuring at low energy is ascribed to "true secondary" electrons which are emitted as a result of cascade processes in the solid [3]. At E(p), the energy of the incoming beam, an elastic peak is observed. This peak is actually comprised of the elastically scattered electrons plus the "quasi-elastic" electrons that have lost a small amount of energy (0.01eV) by phonon scattering. The electrons in this peak are measured in diffraction studies.

Low energy electron diffraction involves observation of the diffraction pattern formed by electrons back-scattered from the surface of the crystal. The electron beams are usually incident perpendicular to the surface. LEED energies are typically between 100 and 1000 eV, with a corresponding wavelength on the order of 1Å given by the de Broglie relationship $\lambda = h/p$. At these low energies the penetration depth of the electrons is only a few atomic layers.

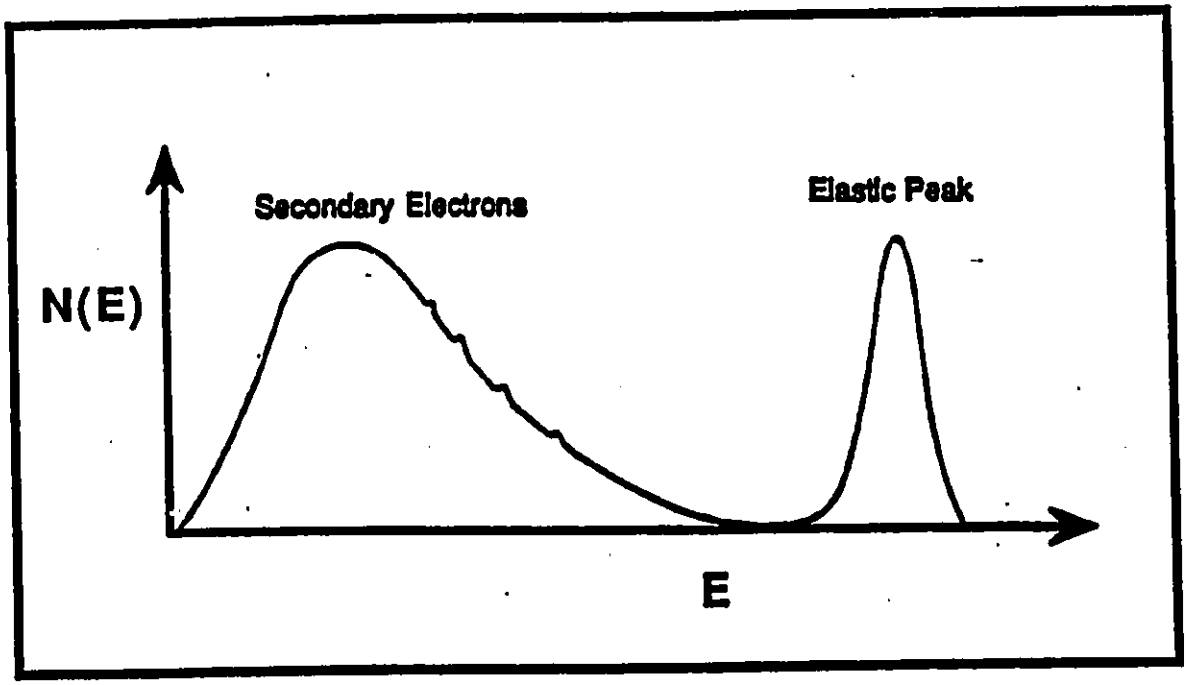

Figure 1. Energy spectrum of a beam of monoenergetic electrons back-scattered from a solid suface

The RHEED geometry is different from that for LEED. The primary electron beam is arranged to have glancing incidence on the surface and electrons scattered at small angles are examined. The momentum transfer in this geometry is only a small fraction of the electron momentum and much higher energies, up to 100keV, are required. From the de Broglie relationship we find that the range of energies 10-100keV corresponds to wavelengths of 0.12-0.037Å. Note that a 50keV electron at an angle of incidence equal to 3° will have approximately the same momentum transfer as a 150eV electron which is back scattered. As well as providing suitable momentum transfers the small angles also ensure that the higher energy electrons incident at glancing angle will not penetrate deeply into the solid.

In a two dimensional array of atoms the periodicity normal to the surface is absent. Hence constructive interference of scattered waves cannot occur in this direction. Since reciprocal space dimensions are inversely proportional to real space distance, we see that to extend real space distance in one direction requires the reciprocal lattice points to move closer together. The conclusion is that extending real space distance to infinity in one direction, as in the case of a surface, generates infinitely long rods in reciprocal space normal to the plane of atoms.

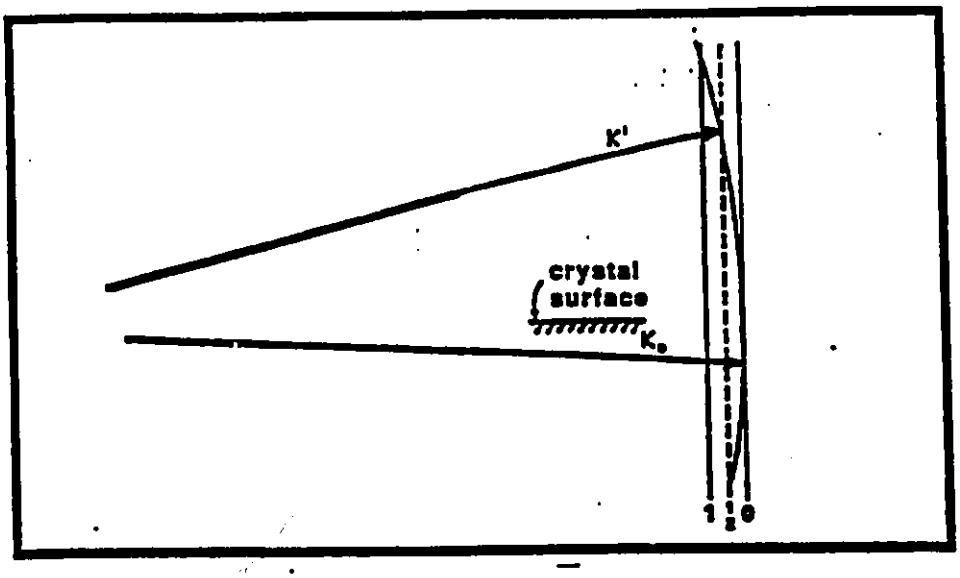

Figure 2a. At high energies the Ewald sphere cuts rods in reciprocal space along their length.

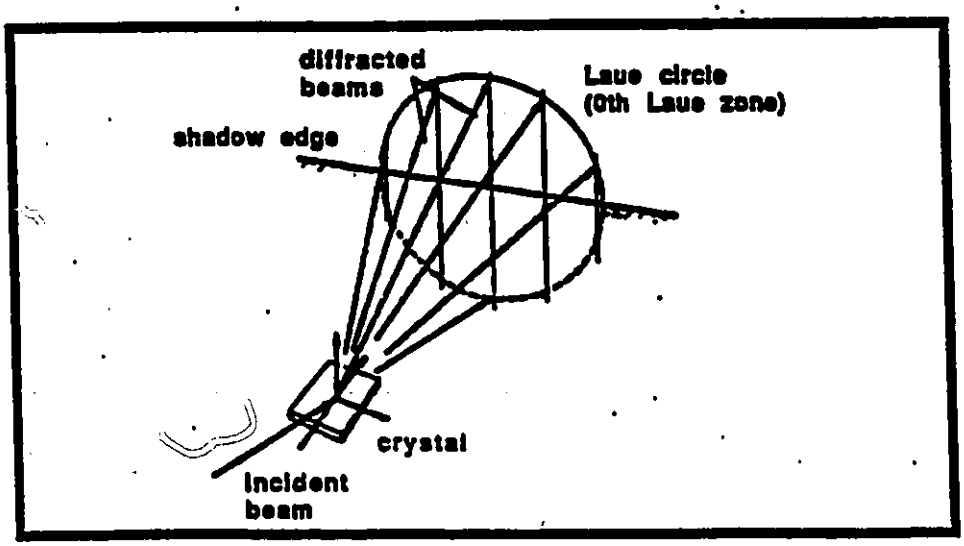

Figure 2b. The 0th Laue zone is formed by the intersection of the Ewald sphere with reciprocal lattice rods.

For high energies, such as 100keV, the electron wavelength is small. The Ewald sphere radius (see appendix) in this case is large compared to typical reciprocal lattice vectors and cuts the rods almost along their length as is illustrated by figure 2. The RHEED pattern will show a set of long streaks normal to the shadow edge of the sample. At lower energies, the Ewald sphere is considerably smaller, and spots are observed in the place of lines. This latter case applies to our situation, in which the energies used were around 5 keV, with a corresponding wavelength of .17Å.

2.1.1 Laue zones

A typical RHEED pattern from a single crystal has a number of characteristic features. The semicircular arcs implied by the sharp spots in the RHEED diffraction patterns are called Laue zones. The brightest arcs relate directly to the underlying periodicity of the bulk structure and are indicated by whole numbers. The atoms at the surface may re-arrange themselves with respect to the underlying bulk, such that the top layer atoms occupy positions at intervals corresponding to multiples of atomic intervals within the bulk. This process is called reconstruction and the diffraction pattern will exhibit fractional semicircular arcs lying between the whole order Laue zones. The zeroth Laue zone refers to the central bright arc. The next bright arc is the

first Laue zone. Any fractional Laue zones present in a RHEED image suggest a re-ordering at the surface.

2.1.1 Kikuchi patterns

A striking feature of RHEED patterns which is useful in determining orientation of the crystal surface consists of dark and light line pairs and bars of varying intensity in the background. Kikuchi lines arise from elastic scattering of electrons which suffer an inelastic collision involving only a small energy loss. The diffuse background is also caused by this kind of secondary scattering, but in the case of Kikuchi patterns these secondary waves are Bragg reflected on a set of lattice planes and are diffracted. A comprehensive treatment of the origin of this phenomena was undertaken by Laue(1935) and Artmann(1944) while a brief discussion of the oversimplified explanation originally proposed by Kikuchi is given in the text by Hirsch et al[4]. The use of Kikuchi patterns together with the spots along the Laue zones provide an excellent method for determining changes in crystal orientation. Kikuchi lines are produced below the surface hence are a characteristic of the bulk.

2.2 Low Energy Ion-Surface Scattering

The composition of crystal surfaces can be analysed by studying the scattered ion spectrum. In the keV range, the observed outgoing ions are produced by single collisions of an incident ion with a target atom. The ions emerging from the surface will have energies that can be predicted by simple binary collision theory.

The energy loss of the primary particle during the collision is assumed to be entirely kinetic. At energies much higher than the thermal energies in the crystal the effect of inelastic processes is minimal and the two body model of elastic collisions may be used to describe the interaction. The elastic binary collision theory assumes that target atoms are free from their neighbours during collisions and that the target atoms are initially stationary before the collision. The laws of conservation of energy and momentum are applied to yield the following relationships between primary ion energy, E_o, and the energy of scattered, E_s, and recoiled, E_r, ions.

$$K_s = \frac{E_s}{E_o} = \left[\frac{\cos\theta \pm \sqrt{A^2 - \sin^2\theta}}{1 + A}\right]^2$$

$$K_r = \frac{E_r}{E_o} = \frac{4A\cos^2\phi}{(1+A)^2}$$

K_s and K_r are, respectively, the scattering and recoil factors. It is evident that these factors are dependent entirely on the scattering angle, Θ, or recoil angle, Φ, and the mass ratio A = target mass/incident mass.

Since the de Broglie wavelength of the incoming particles is much smaller than the spacing of the atoms at the surface a quantum approach was not necessary. For a non-relativistic particle the following relations are true:

$$p^2 = 2mE$$

$$\lambda = \frac{h}{p} = \frac{h}{\sqrt{2mE}}$$

Thus for 10 keV oxygen ions $\lambda = 2.3 \times 10^{-13}$ m, which is much smaller than the atom spacing. For Silicon the lattice constant is 5.431Å.

The characteristic peaks of the energy spectrum correspond to energies of scattered and recoiled ions. The masses of the target atoms can be determined by referring to graphs of K factors as a function of scattering angle shown in figure 3. The ratio of the peak energy to the incoming ion energy, the K factor, and the scattering angle will identify a point on the graph. The intersection of this point with the curve corresponding to a particular mass ratio, A, along with knowledge of the incoming ion mass will determine the mass of the target atom. In this way the composition of the surface can be monitored.

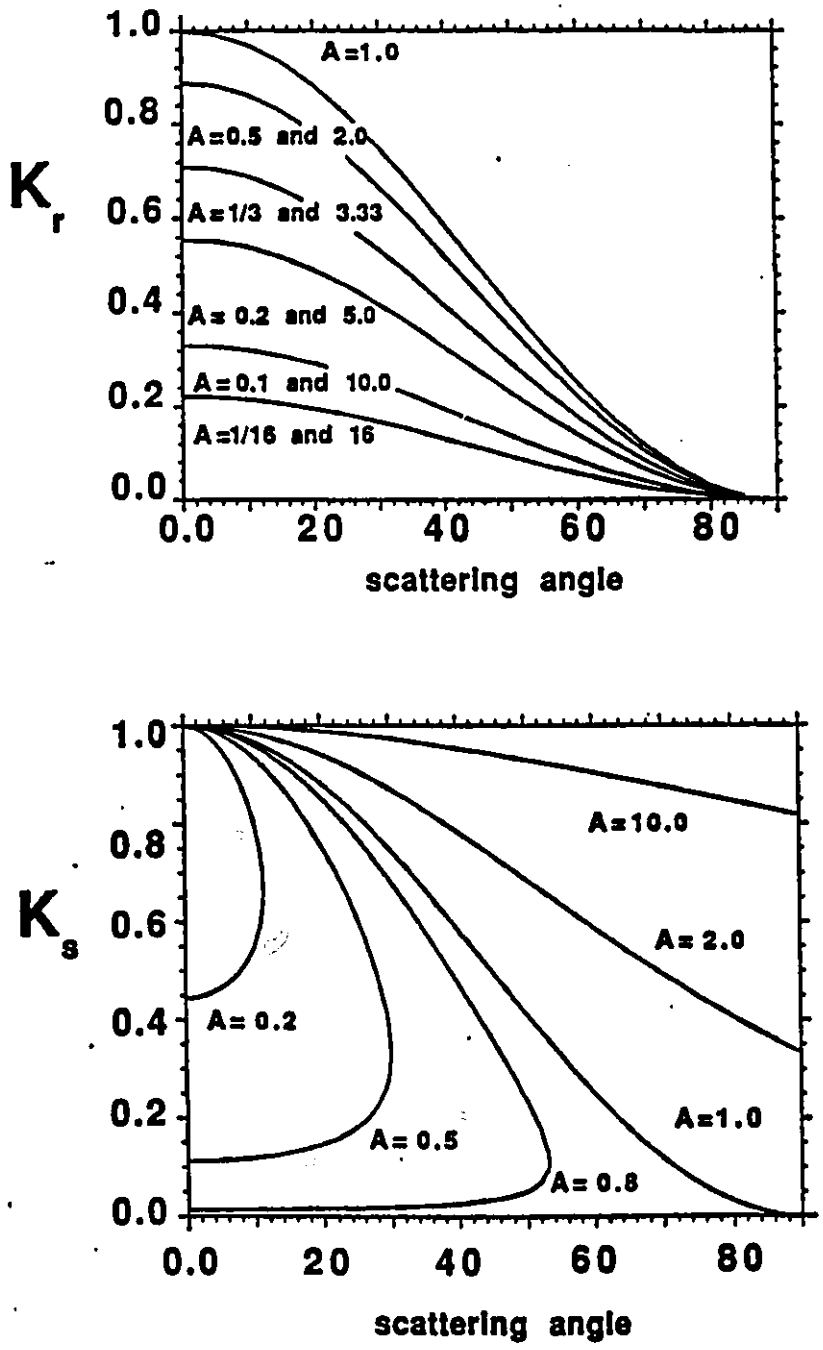

Figure 3. Graphs of K-factors as a function of scattering angle for various values of A.

Chapter 3. Si bulk and surface crystallography

Silicon crystallizes in a diamond structure, which is composed of two face centred cubic lattices displaced from each other by one-quarter of a body diagonal. Figure 4 shows a diagram of the diamond structure indicating the bulk equilibrium positions of the atoms. Figures 5a and 5b show the bulk equilibrium positions of the atoms in two low index planes. These are idealized structures that serve as points of reference when describing the rearrangement of atoms which occurs at the (100) and (110) surfaces of Silicon. This rearrangement phenomenon, in which the surface symmetry is different from that of the underlying bulk, is called reconstruction, and is the result of a long range order at the surface which does not exist in the bulk.

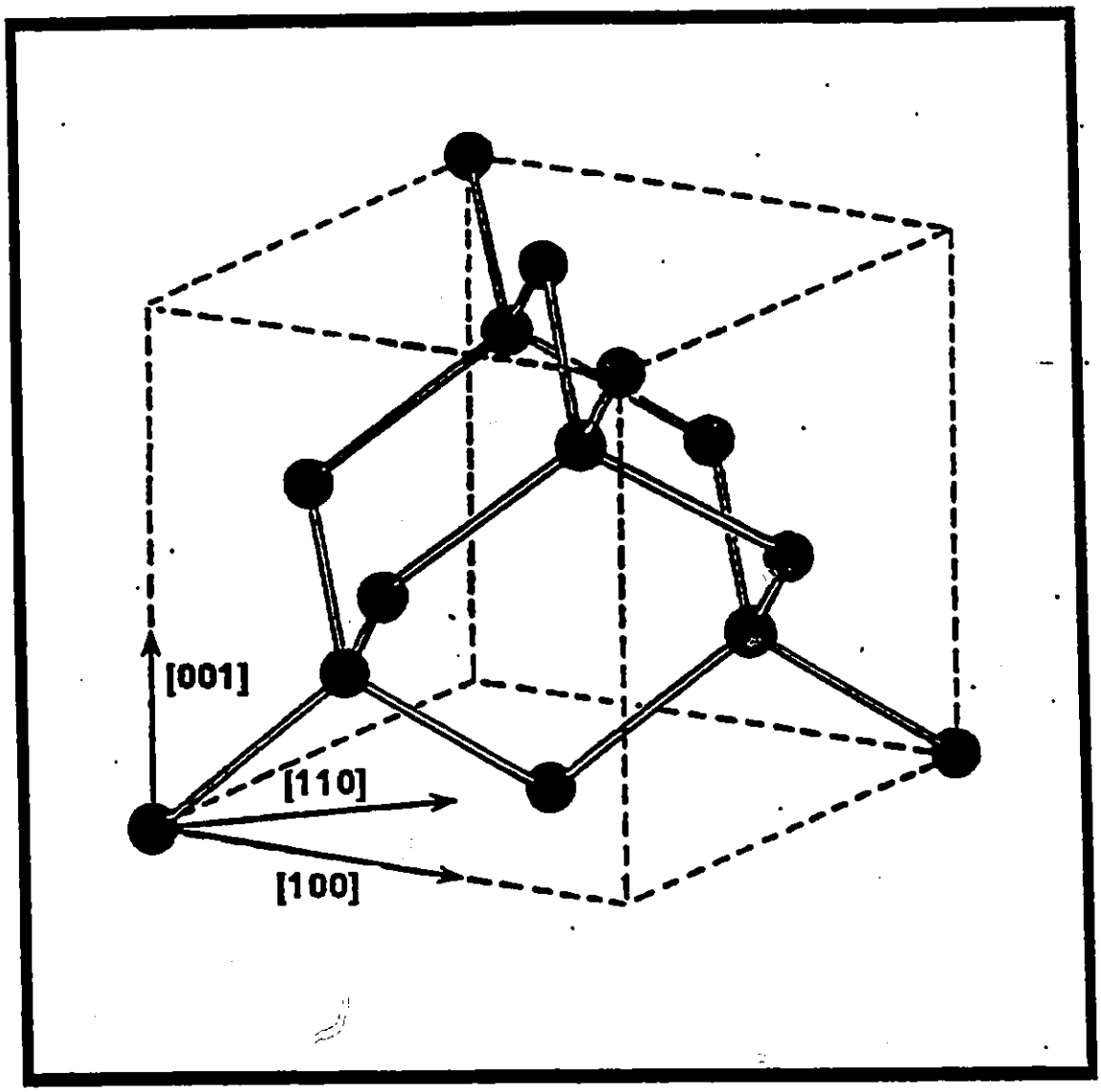

Figure 4. The diamond crystal structure.

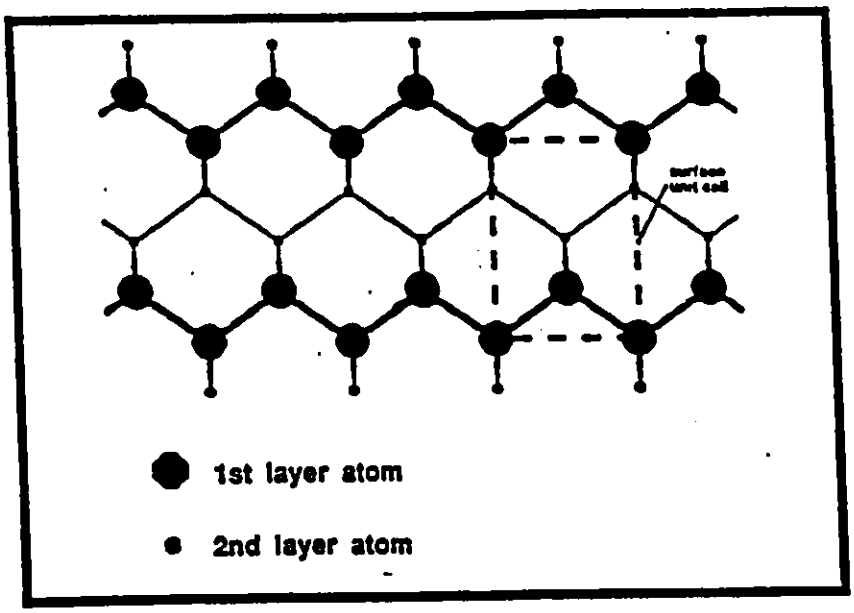

Figure 5a. The bulk-exposed (110) plane of Silicon.

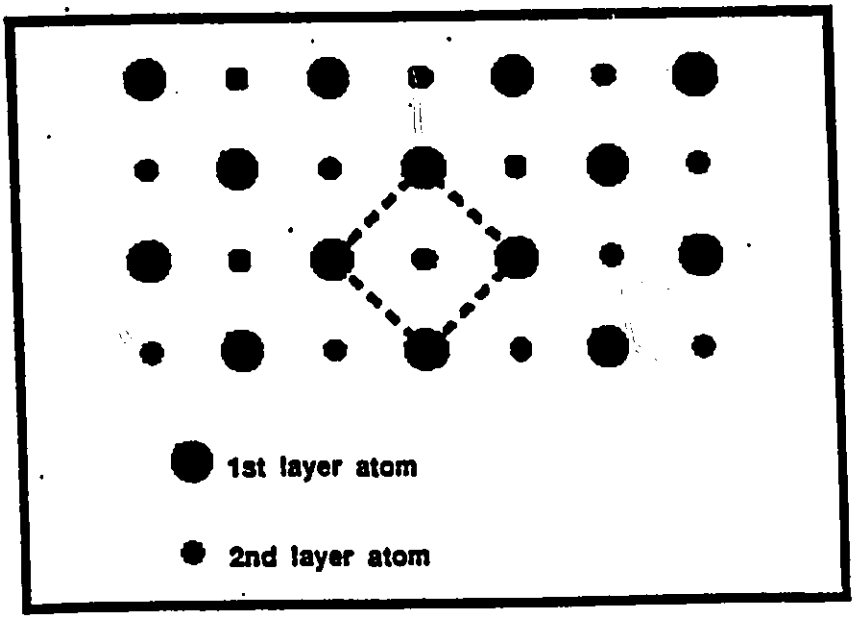

Figure 5b. The bulk-exposed (100) plane of Silicon.

RHEED and LEED patterns of the reconstructed Si(100) surface exhibit a doubling of the periodicity along the [110] or [$\bar{1}$10] direction. The reciprocal lattices of the two orthogonal domains with the 2x1 unit mesh are shown in figure 6b. The observed reciprocal lattice in the RHEED pattern consists of a superposition of these two. This 2x1 structure has been used as the characteristic identifying feature of the reconstructed Si(100) surface since the late 1950's[5,6,7].

Diffraction experiments suggest four different surface structures formed at the Si(100) surface[8] (for a discussion of the vocabulary of surface crystallography see appendix 2):

i) Si (100) (2x1)

ii) Si (100) c (4x2)

iii) Si (100) p (2x2)

iv) Si (100) c (2x2)

It is suggested that a mixture of (2x1), c(2x2), p(2x2) and c(4x2) structures can be expected on every clean Si(100) structure. The ratios may depend on annealing history of the sample. However the (2x1) is the most commonly reported surface structure at Si(100).

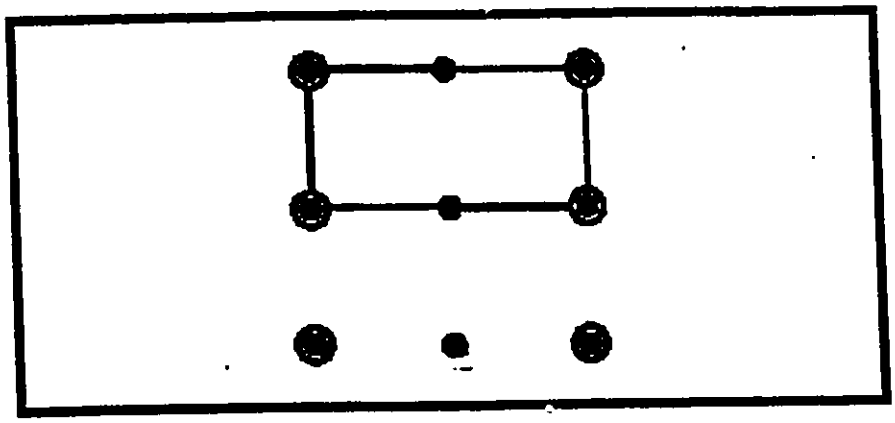

Figure 6a. The 2x1 reconstructed Si(100) unit cell in real space.

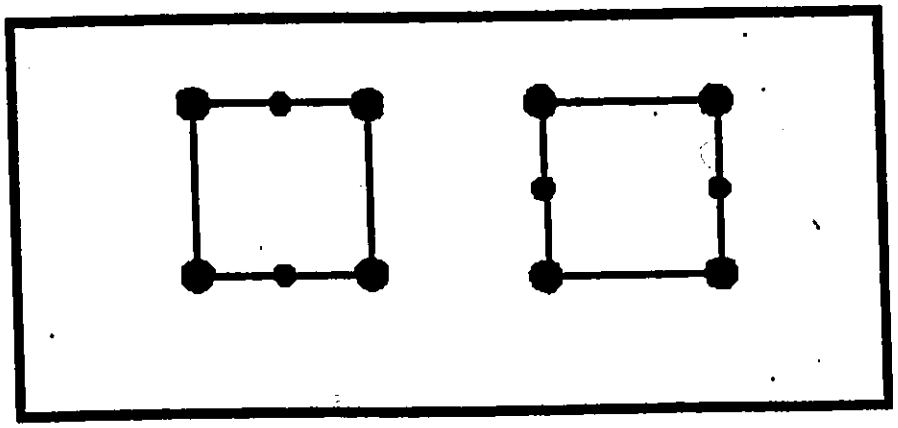

Figure 6b. Two Si(100) unit cells in reciprocal space, rotated at 90° with respect to each other.

A number of structures have been reported at the clean Si(110) surface. Early studies reported various surface structures which were caused by both reversible and irreversible phase transitions occurring at different temperatures on a clean surface[9,10]. In 1985 Ichinokawa et al[11] found a strong relationship between the amount of nickel found on the surface and the resulting reconstruction. It has been reported by Van Loenen et al that traces of Cu at the surface also affected the surface structure. The observed phases induced by nickel or copper impurities have been grouped into three categories[12]:

i) The (2n x 5) phases, e.g. (2 x 5) or (4 x 5), which exist below 600°C. The 2n x structure is along [001] and the 5 x structure is along [1$\bar{1}$0][13].

ii) The (2 x 1) structure which exists between 600°C and 750°C. The doubling occurs along the [001] direction.

iii) The ((2n+1) x 1) phases , e.g. (5 x 1), (7 x 1) and (9 x 1), found at temperatures higher than 750°C. The 2n+1 structure forms along [001].

It has been shown that only a "16 x 2" and a "32 x 2" phase exists at the clean Si(110) surface[14]. These are oblique

structures shown diagramatically in figure 7. The surface is made up of alternating high and low terraces with edges aligned along the [1$\underline{1}$2] and [1$\underline{1}\underline{2}$] directions. The surface must be extremely clean in order to observe such structures: samples contaminated with as little as 0.007 monolayers of Ni will not show the 16 structure.

Fractional order spots have been observed to disappear when hydrogen is adsorbed onto the Si(100)2x1 surface[15]. This "dihydride" phase can be converted to the (2x1) "monohydride" phase by heating the sample. A recent experiment by Ampo et al[16] suggests that a similar effect may occur at the hydrogenated Si(110) "16x2" surface.

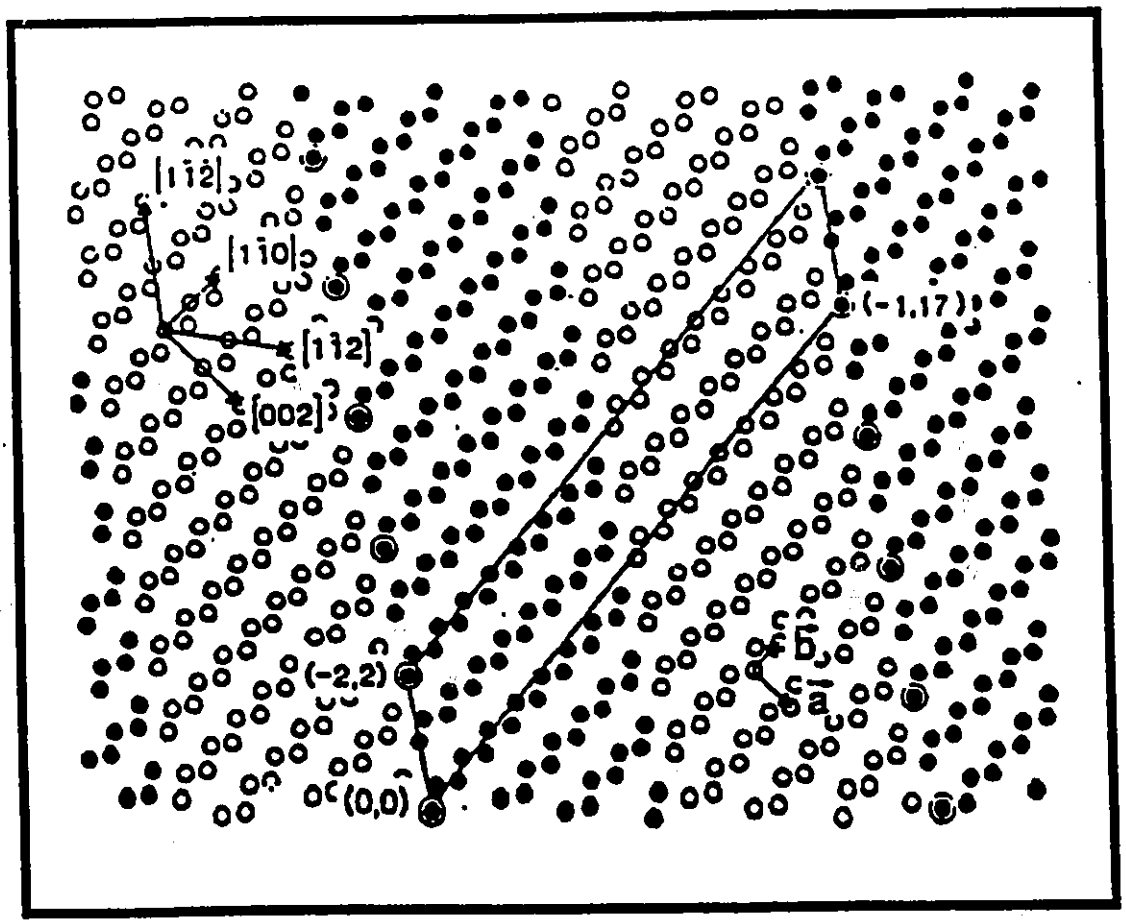

Figure 7. The Si(110) "16x2" reconstructed unit cell in real space.

Chapter 4. Instrumentation

4.1 Vacuum requirements

The UHV chamber is coupled to the ion source via a number of pressure steps which may be isolated from one another. The accelerator section pressure is maintained at 10^{-6} torr. Though not UHV the mean free path is several kilometers at this pressure, so that gas scattering is small. This is achieved by two 100 l/s diffusion pumps backed by a common rotary pump. O- ring seals are used on this part of the beam line.

Ionization gauges are used to measure the pressures in the various sections, and thermocouple gauges monitor the pressure in the rotary pumps which back each diffusion pump.

The differential section isolates the "dirty" vacuum of the accelerator section from the "clean" ultra-high-vacuum chamber. A pressure of 4×10^{-9} torr is maintained by a 200 l/s diffusion pump with a special UHV cold trap. The full UHV technique was used in the construction of this section and copper gaskets were used as

seals. The use of copper gaskets avoids the release of organic contaminants and allows baking. After opening to atmosphere an overnight bake is necessary for both this section and the UHV section. Both sections are constructed of bakeable stainless steel. Baking releases condensed water vapour and other gases which have been adsorbed on the walls of the chamber which can then be pumped away. It was found that the differential section was so clean that after baking this very good pressure was maintained without using liquid nitrogen in the cold trap.

Materials which were used in the construction of the UHV chamber were chosen to avoid high vapour pressures. Stainless steel, molybdenum, and tantalum are used for mechanical parts. Oxygen free high conductivity copper is used as a conductor. Materials used as insulators include glass, sapphire and high density ceramics such as alumina. The only plastic material which combines the low vapour pressure with high temperature stability is teflon.

A base pressure of 2×10^{-10} torr was achieved in the UHV chamber using a 415 1/s diffusion pump with a liquid nitrogen cold trap and a titanium sublimation pump with cold plate. The backing pressure was provided by two rotary pumps which also back the differential section. Since this section must be bakeable,

rubber O-rings cannot be used as seals. A viton O-ring in the poppet valve between the chamber and the diffusion pump limits the baking temperature to 300° C. It has been found that viton cannot be used to make vacuum-atmosphere pressure seals, but it is appropriate for isolating different vacuum sections. The titanium sublimation pump is activated prior to the taking of measurements in order to achieve the best possible vacuum. The time available to take meaningful measurements is directly related to the pressure in the chamber. At 2.5×10^{-10} torr one monolayer of atoms is expected to stick to the surface in 4000 seconds assuming a sticking probability of one. The UHV chamber can be isolated from the differential section by closing a 45° valve.

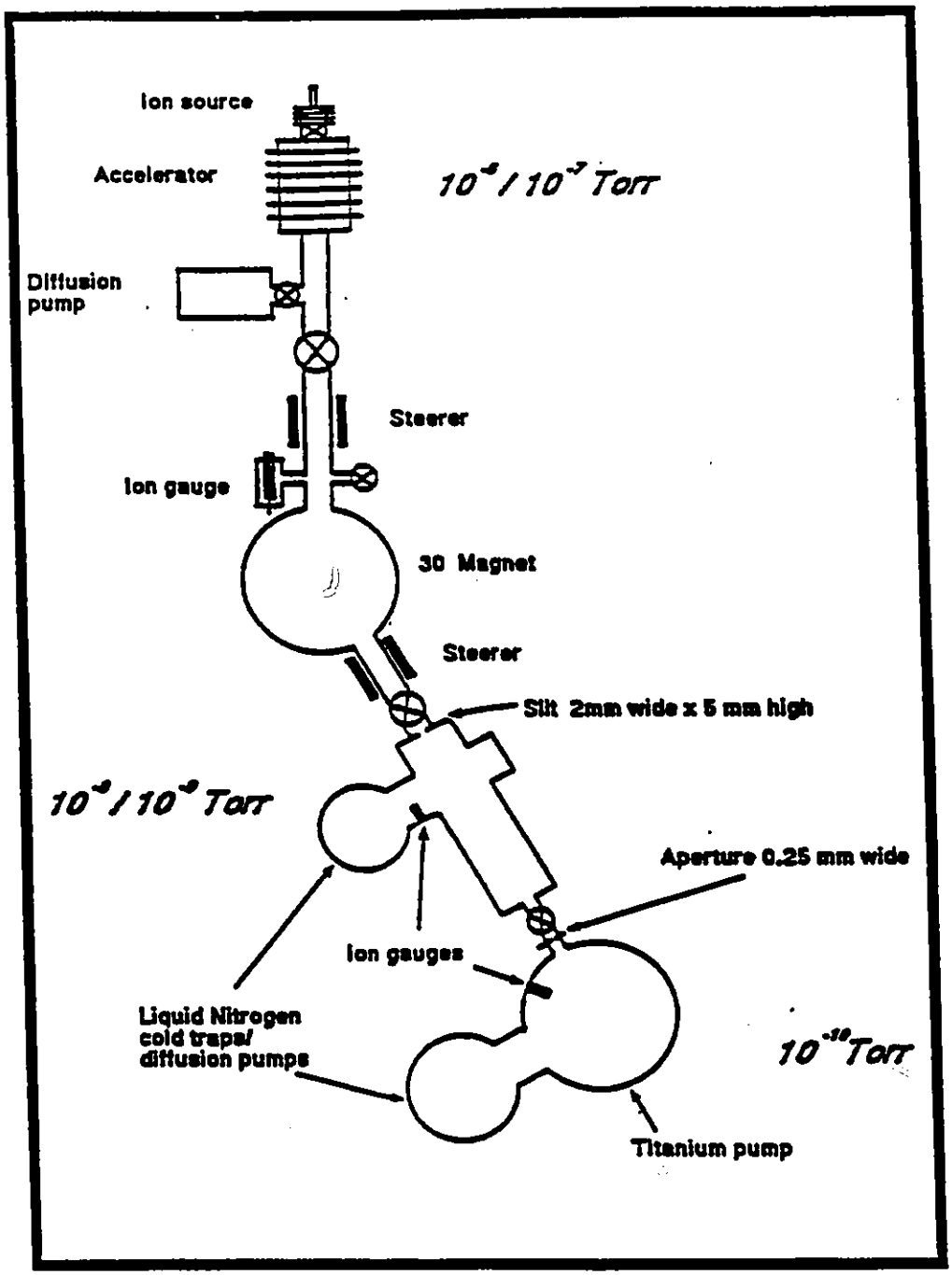

Figure 8. The ion beam line, indicating regions of different pressure.

4.2 Ion beam production and transfer

Oxygen gas is ionized in a radio frequency ion source capable of producing a flux of ions on the order of microamps. A discharge in a cylindrical glass tube filled with gas is stimulated by the surrounding exterior electrodes of a high frequency RF oscillator. The plasma inside the tube acts as a conductor. An anode electrode set into the glass attracts electrons while positive ions are accelerated towards the only other conducting material in the tube, the exit canal. Because of the much higher mobility of the electrons the potential of the plasma is close to that of the anode. Inside the canal the ions encounter a nearly field free region.

Both positive and negative ion beams can be produced. A process of electron capture can occur inside the canal caused by the residual gas, forming negative ions from positive ions. Inverting the beam polarity requires the reversal of all electric fields except in the ion source. Beyond the exit canal is a region of much lower pressure, where the ions are extracted by a strong electric field. The mean free path is large enough that the ions retain the charge state which they had at the canal exit.

The ions emerge from the field free region of the exit canal into a region of nearly uniform electric field. The fringe field between the two regions provides the focusing of an electrostatic positive lens so that the beam can be converged to a small diameter beyond the accelerator. The energy of the ions should in theory equal the ion charge multiplied by the sum of the anode potential plus the accelerator voltage. This seems to occur for positive ion beams but for negative ions it was observed that the energy was determined only by the accelerating voltage. The anode potential was in the range of 0-2.5 kV while the accelerator voltage output was between 0 and 150 kV. Beam currents obtained for the negative ions were found to be much weaker than those obtained using positives.

Separation of ions according to mass occured in a 30° deflection magnet. Beam selection is made by observing a spectrum of peaks corresponding to different masses as the magnetic field is varied. The selected ion beam is deflected towards the differential section. Two magnetic steerers which can deflect the beam a few degrees guide the beam, one on either side of the magnet. These each provide transverse magnetic fields of a few hundred gauss over a 20 cm length.

An aperture, electrically isolated from the stainless steel beam line, separates the accelerator section from the differential

section and another aperture separates the differential section from the UHV chamber. These apertures serve to control the gas flow between regions of different pressure. They are also necessary in order to collimate the beam both in position and direction. Currents produced by the ion beam striking the apertures can be measured, providing a way of optimising the beam transmission from ion source through to the target.

4.3 ESA and CEMs

The scattered ions are energy analyzed using a $\pi/\sqrt{2}$ electrostatic analyser (ESA). This consists of two $\pi/\sqrt{2}$ cylindrical sector electrodes with grounded plates at each end containing entrance and exit slits. A radial electrostatic field is set up by applying opposite voltages to the cylindrical electrodes. At a particular voltage setting, the ESA can transmit only those ions with an appropriate E/q. Neutrals are not deflected and therefore not detected. In this way a certain energy range can be scanned for particles.

The ions which have suitable trajectories to pass through the ESA are detected by a channel electron multiplier (or CEM). The efficiency of CEMs is independent of energy between 2 and 10 keV. Below 2 keV the secondary emission coefficient of the CEM material decreases which means that there is a low chance of a secondary electron being captured and multiplied. Above 10 keV the ion range is high enough that again the surface secondary electron emission is less.

A second CEM was included in the chamber in direct line of sight of the sample. This allowed us to measure the actual ion flux on the target during measurement, which provided information used to normalize the energy analyzed counts as well as allowing

us to take beam fluctuations into account. Current measurement on the sample was found to be ill suited to the experiment because of false current readings due to thermionic emission effects after the sample was heated, and the difficulty of measuring these fluctuating very small currents accurately.

The output of the CEMs is digital. The pulses were amplified and counted by scalers. The output of both CEMs was recorded on a computer, together with the ESA voltage which was incremented in small steps by computer controlled power supplies, so that an energy spectrum was produced automatically.

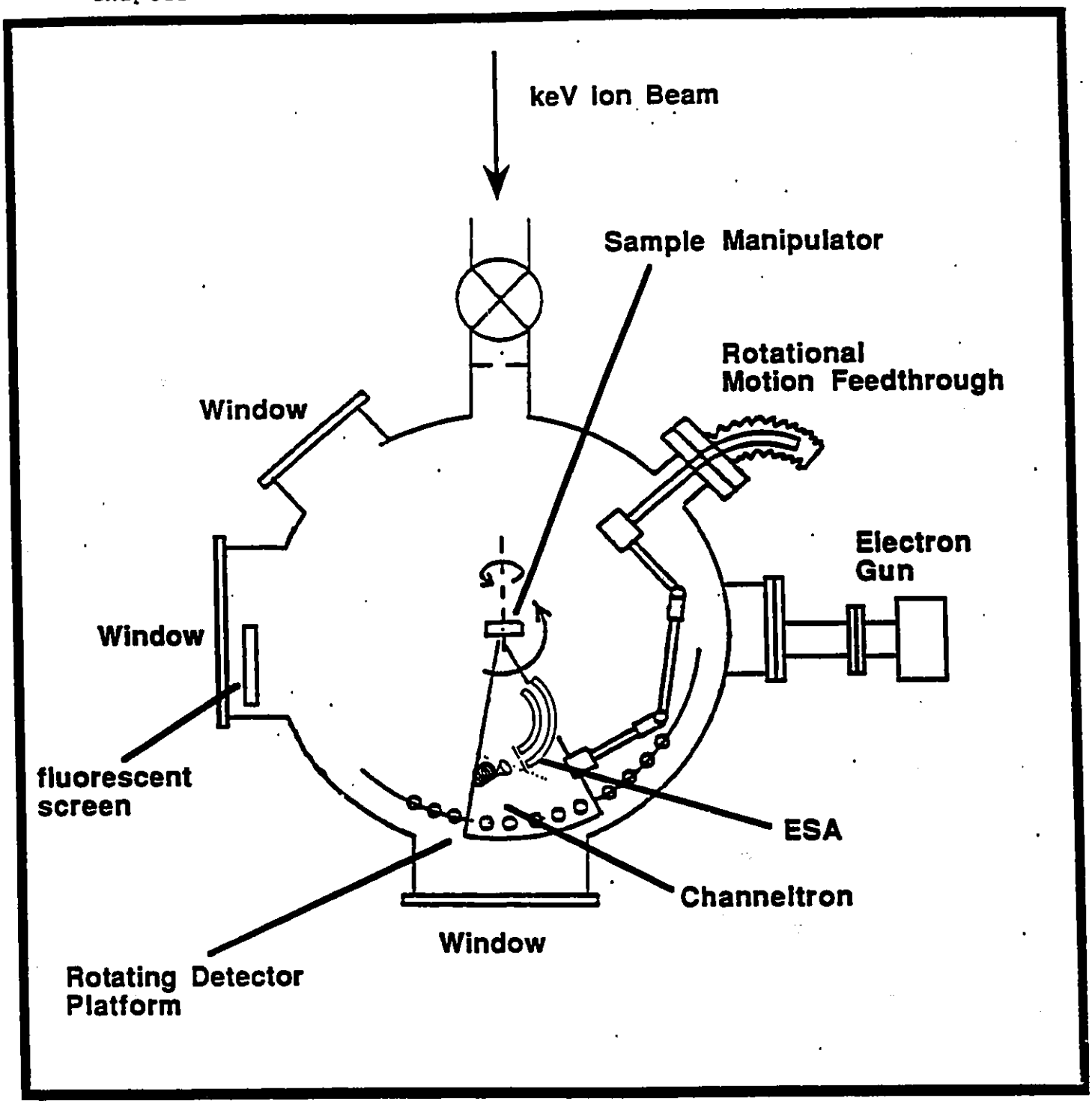

Figure 9. UHV chamber geometry.

4.4 Sample Manipulator and Heater

The sample manipulator locates the sample at the centre of the UHV chamber. Molybdenum clamps secure the sample in place on a backplate which is also made of molybdenum. The manipulator provides x, y, and z translation, rotations in the azimuthal plane and allows us to vary the polar angle of the incoming beam, giving five different movements in all.

Current produced by a beam hitting the target is measured using a Keithley picoammeter. The ion beam into the chamber has a width of 0.25 mm. The collimated beam has a narrow energy spread and an angular spread of about 2mrad at the target.

An electron beam heater is included, behind the sample, providing up to 1300°C of heating. The thermionic emission filament is isolated from the manipulator and held between two pairs of insulating rods made of alumina. Originally 200 V was supplied to the filament which produced about 110microamps of electron current on the back plate to heat the sample. A problem was encountered. It was observed that a dramatic rise in pressure accompanied the heating of the target. The effect was due to stray electrons produced by the filament escaping from the heater and striking the inner walls of the chamber causing desorption, mainly of hydrogen. The solution involved biasing

the anode (target) positively and grounding the filament. The electrons from the filament were then at the same potential as the chamber so that there would be no attraction. The drawback to this set-up is that thermocouples cannot be used to monitor the temperature of the specimen as they require a grounded surface in order to operate.

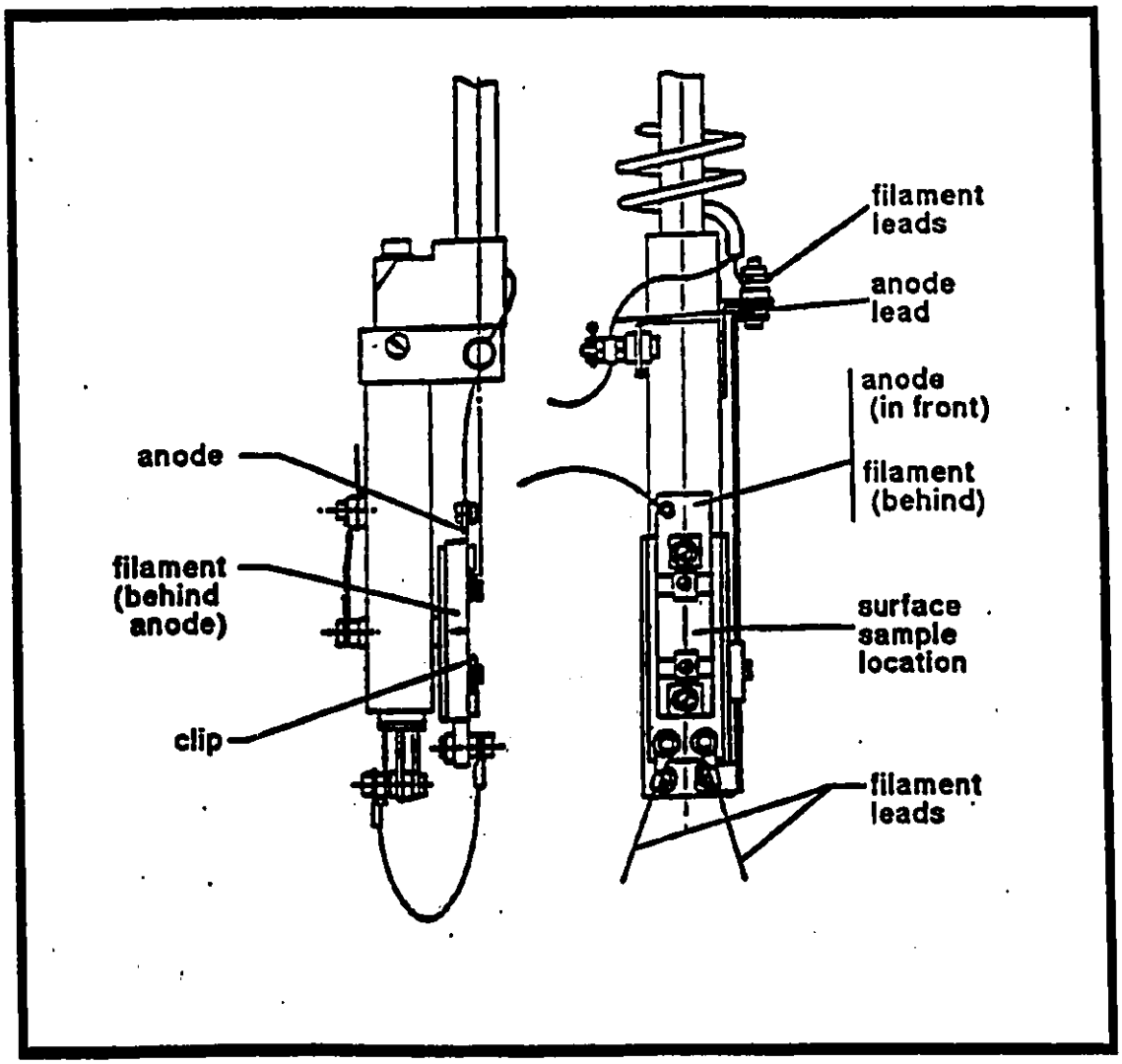

Figure 10. The electron beam heater and sample holder.

4.5 Controlled Contamination

In certain cases it is desirable to introduce foreign atoms or molecules into the environment of the sample. We were able to control the rate at which foreign gases enter the UHV chamber via a stainless steel leak valve. A mass spectrometer was used to identify the impurities in the chamber.

This situation was encountered when the target was cleaned by sputtering. This technique will be discussed in a later section. A sputter gun pointed down at 45° towards the sample. The position and orientation of the sample relative to the sputter gun were adjusted using the specimen manipulator.

In our attempt to reproduce the Si (100) (1x1) - H structure hydrogen gas was slowly admitted into the chamber through the leak valve until a pressure of 5×10^{-6} torr was achieved. The electron gun filament and sputter gun filament were turned on in order to dissociate the hydrogen molecules, providing hydrogen atoms which would then adsorb onto the surface.

4.6 Sample cleaning

The principal material of interest was the mirror polished (100) surface of an N-type silicon wafer of thickness 356 - 406 microns and resistivity 1.00 - 2.00 which was cut to a rectangular piece about 1cm x 2cm. The wafers used have a protective oxide coating, about 0.1 microns thick, which must be removed in order to expose the clean silicon surface. The samples were provided by and oxidized at the Microstructures Laboratory at NRC. The oxidation process involves exposing the silicon wafer to ozone gas in an oven for about an hour. A variety of cleaning procedures were investigated and two typical methods are discussed below.

Sputtering involves bombarding the surface of the specimen with energetic ions, thereby stripping away the surface and leaving a disordered bulk exposed plane. The resulting surface is free from contaminants other than those remaining from the sputtering, but in the process surface order is destroyed and an amorphous surface results. Subsequent heating, anneals the material so that the surface atoms reorder.

The SiO, having a higher vapour pressure than Si, could be removed by heating the specimen to about 1250°C for a few seconds followed by continuous heating at 850°C for 15 to 20 minutes.

The resulting surface seemed to be equivalent to one which had been sputtered using 2 keV argon ions for 15 to 30 minutes and then annealed at about 1000°C for 15 minutes. The stress experienced by the sample is less at these lower temperatures hence there is less chance of the sample fracturing. In addition, the mechanical parts in the vicinity of the sample are not heated to such high temperatures for extended periods of time limiting both outgassing from the sample holder and damage induced by heat stress.

Chapter 5. Detailed RHEED operation

A RHEED system consists of an electron gun, a specimen manipulator and a device for displaying and recording the diffraction pattern. Since the pressure inside the chamber was in the 10^{-10} torr range gas discharge was unlikely and the probability of scattering of electrons by residual gas particles was negligeable. RHEED systems are much easier to build than are LEED systems. However in some UHV chambers the geometry is restricted so that it is not possible to measure grazing angles and LEED must be used. A LEED system requires a hemispherical fluorescent screen with an aperture in the centre between the electron gun and the sample. The backscattered electrons are then observed on the screen. Such systems are now available commercially. Our system allowed the measurement of grazing angles so that the simpler RHEED system was constructed.

The RHEED system operated perpendicular to the ion beam line so that the two geometries did not interfere with each other and the manipulator was used to adjust the sample into position for either of the two beams.

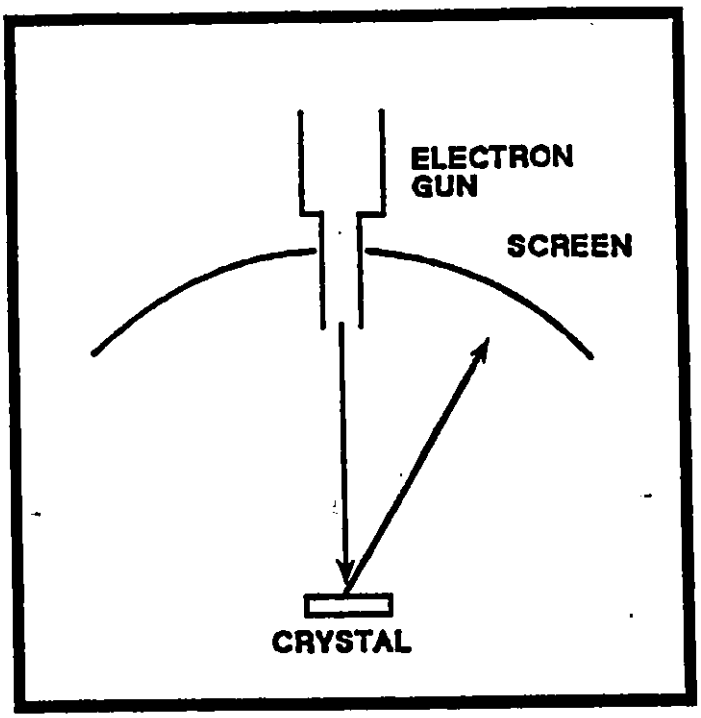

Figure 11a. LEED geometry.

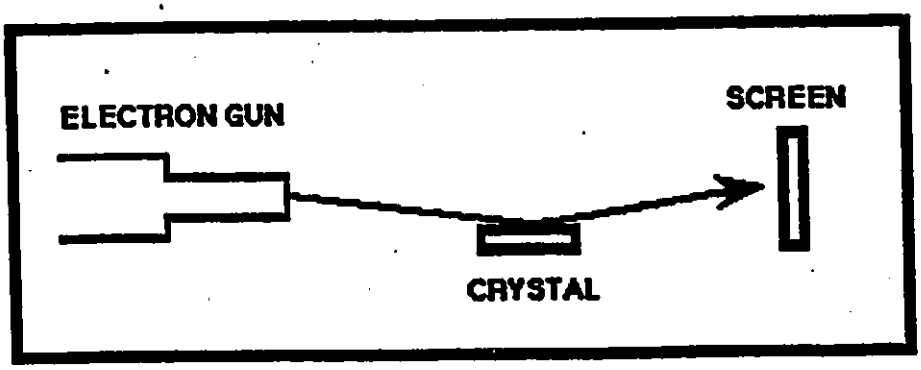

Figure 11b. RHEED geometry.

The RHEED system was designed and constructed in the laboratory. A commercially purchased electron gun was used. This was probably mass produced as a component of a cathode ray tube, but proved ideal for our requirements. The layout of the electrodes is included in fig. 12 The filament, specified to be run between 2-2.5 volts at 3-3.5 amps was supplied from the main AC power line using a 45:1 step down transformer, providing a maximum of 2.5 VAC. This value could be reduced by means of a Variac. Since the filament supply was required to be at the high voltage a 1:1 isolation transformer rated to 15 kV was used. The filament was centre-tapped to provide a negative biased voltage and remove the AC ripple. This DC voltage was supplied by the 10HARD1-1 highly regulated encapsulated commercially manufactured power supply. From this power supply were derived all the voltages required for the electron gun, by means of the voltage dividing circuit illustrated in fig 13. Thus the requirement of having a focus electrode voltage 25%+/-5% of the accelerator voltage was achieved.

The accelerating voltage could be between 200eV and 10keV as specified by the electron gun manufacturer. We used values around 5keV. This upper limit was determined by the voltage rating of the MHV connectors at the output of the power supply. These are rated at a maximum of 5kV and should be used with lower voltages. At higher settings sparking occurred.

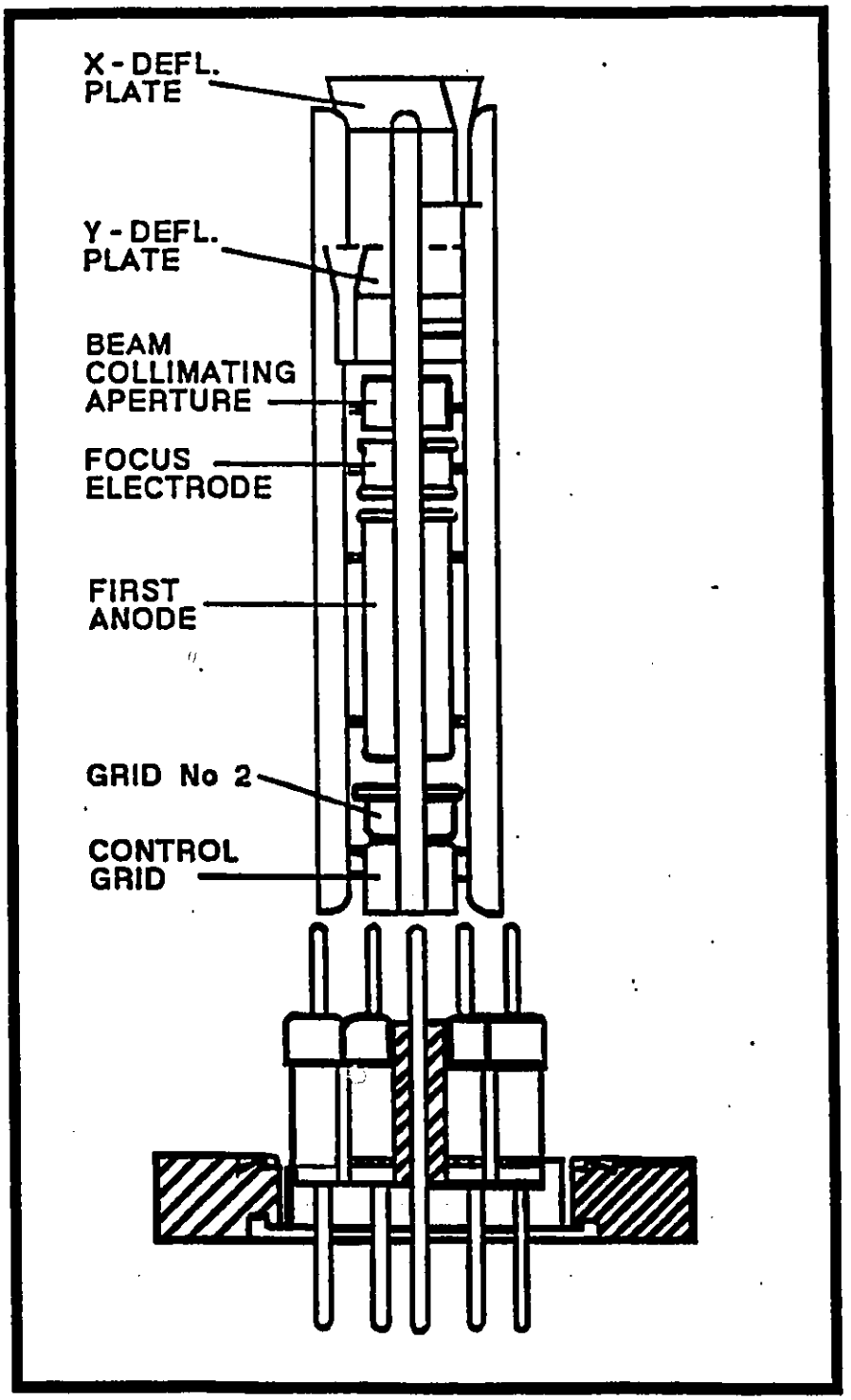

Figure 12. Layout of the electron gun electrodes.

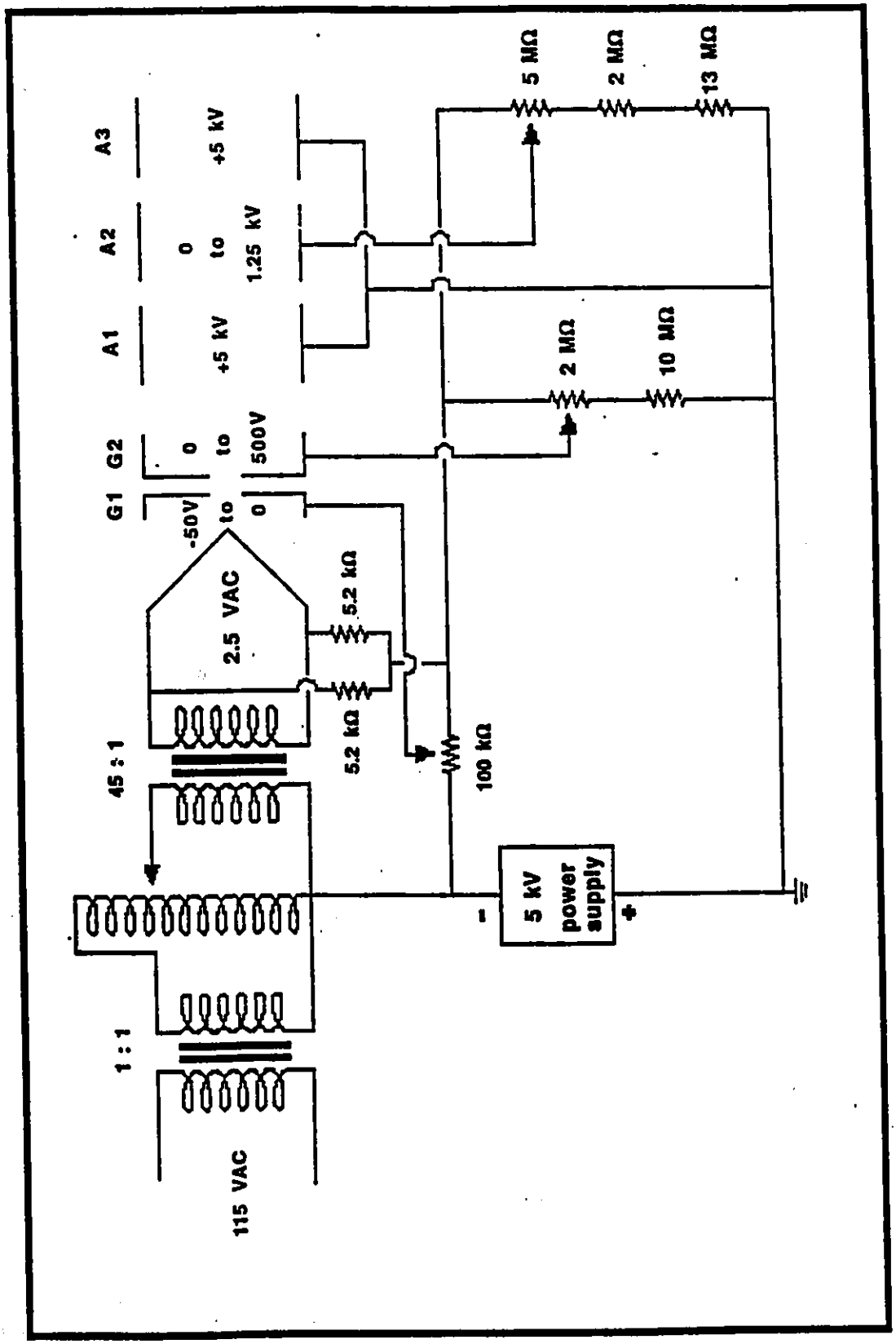

Figure 13. Voltage divider circuit for the electron gun.

Multiwire cables were not readily available to withstand high voltages so many separate coaxial cables were used. A particular difficulty was encountered with the filament supply which also carried a large current (2A). Initially it was found that there was too much voltage loss in the cables, so the step-down filament transformer was transferred to the electron gun base. It had to be well insulated from the surrounding shield, since it was at the high accelerating voltage. A chassis box at the base of the electron gun was used to contain connections for the cables carrying voltage from the power supplies to the electrodes of the gun. The space inside the box was constricted and the various connections carrying high voltage had to be well insulated from one another. Ignition wire was found to provide adequate insulation and good conduction.

In order to view the electron diffraction pattern the elastically scattered electrons were incident onto a fluorescent screen. Preliminary tests using fluorescent screens which had been cut from CRT's showed that the phosphor of short persistence screens could be used. The fluorescent powder was easily damaged but survived exposure to air and gave adequate light output. A number of these fluorescent screens have been used, and all have worked successfully. One was ruined when a silicon target was melted by overheating. The phosphor probably coated with a layer of evaporated silicon. The screens were cut into half disks and

placed in the port of the UHV chamber covered by a window. This allowed us to see a RHEED image as well as giving us a view into the chamber.

A spot size of approximately 0.5mm. diameter was obtained at a distance of about 15cm. from the sample after suitable adjustment of pre-accelerator, grid and focus voltages. Once the desired spot size was obtained the controls were left at those settings. The position of the spot could be adjusted via x- and y-deflector electrodes at the end of the electron gun. A DC regulated power supply was built to supply between 1.5 and 70 V to the deflection electrodes as shown in figure 14. This allowed us to move the spot through a 1 cm. distance at the screen. A combination of adjusting the sample position and spot position was used in order to obtain a RHEED image that allowed the maximum possible number of Laue zones to be seen.

The field produced by the electron beam heater caused the electron beam from the gun to deflect away from the target so that RHEED images could not be obtained during heating. An ungrounded target was found to charge-up during heating so that once again RHEED measurements could not be made even after the heater was turned off. By grounding the target the image could be obtained.

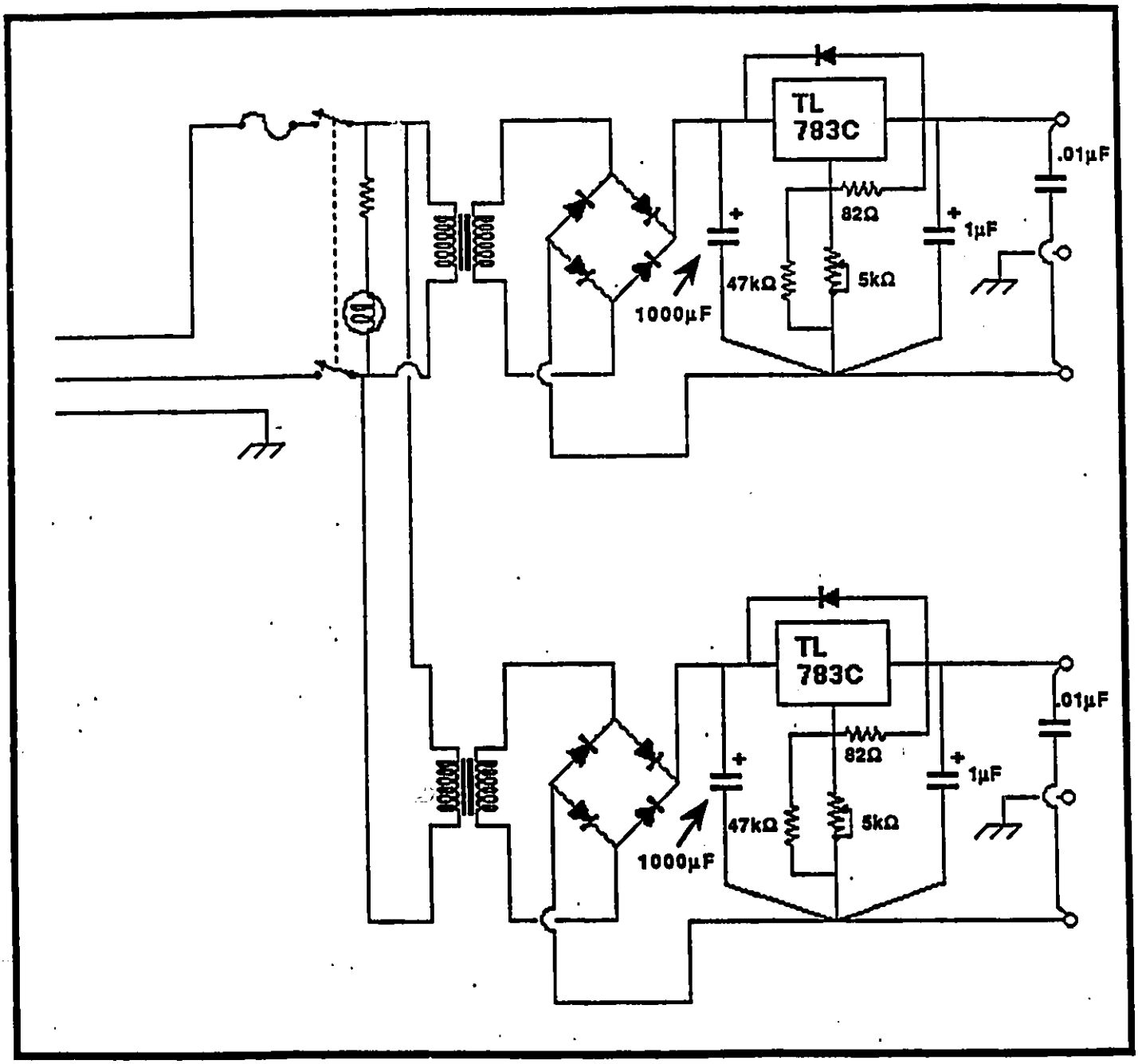

Figure 14. Deflection electrode power supply.

Chapter 6. Experimental Results

6.1 Si(100)

The RHEED image we obtained of the clean Si(100) surface was independent of the procedure used to clean the sample. Whether a combination of sputtering and annealing, or heating to high temperatures was used to remove surface contamination, the electron diffraction pattern clearly exhibited the expected 2x1 reconstructed arrangement. Figure 15 shows two photographic images of the pattern visible on the fluorescent screen. The images on the photographs represent diffraction patterns obtained for electron beams incident at different azimuths. In the first, there was a doubling of the periodicities along and perpendicular to the whole order Laue zones. There appeared single faint arcs of spots between the strong arcs, while along the intense arcs we observed an alternating sequence of strong and weak spots. A second symmetric pattern was obtained by rotating the sample 45° about its azimuth. Hence the unit cell of the surface should appear rotated about 45° as well. Figure 16 indicates how the reconstructed unit

cell can be extracted from the RHEED images. Since the doubling of periodicity occurs along the edges of the unit cell, which correspond to the <110> directions, we conclude that the first image corresponded to the electron beam incident along a <110> direction, while in the second case the crystal surface was oriented along a <100> direction with respect to the electron beam.

In the first case the beam was aligned with the direction of a cleavage edge of the wafer. Hence we could conclude that the wafer cleaved along <110> directions. This was the expected result, since it is well known that Silicon cleaves along {110} and {111} planes. Since a <111> direction is not included in the (100) plane, the cleavage must occur along a <110> direction.

The Kikuchi patterns, which can be seen in the photographs, were used as a visual aid in aligning the crystal so that the electrons traveled along a major crystallographic direction. A slight change, say 1.5°, in orientation would cause the Kikuchi pattern to translate away from the centre of the image, whereas the deviation in the position of the diffracton pattern could be too small to notice.

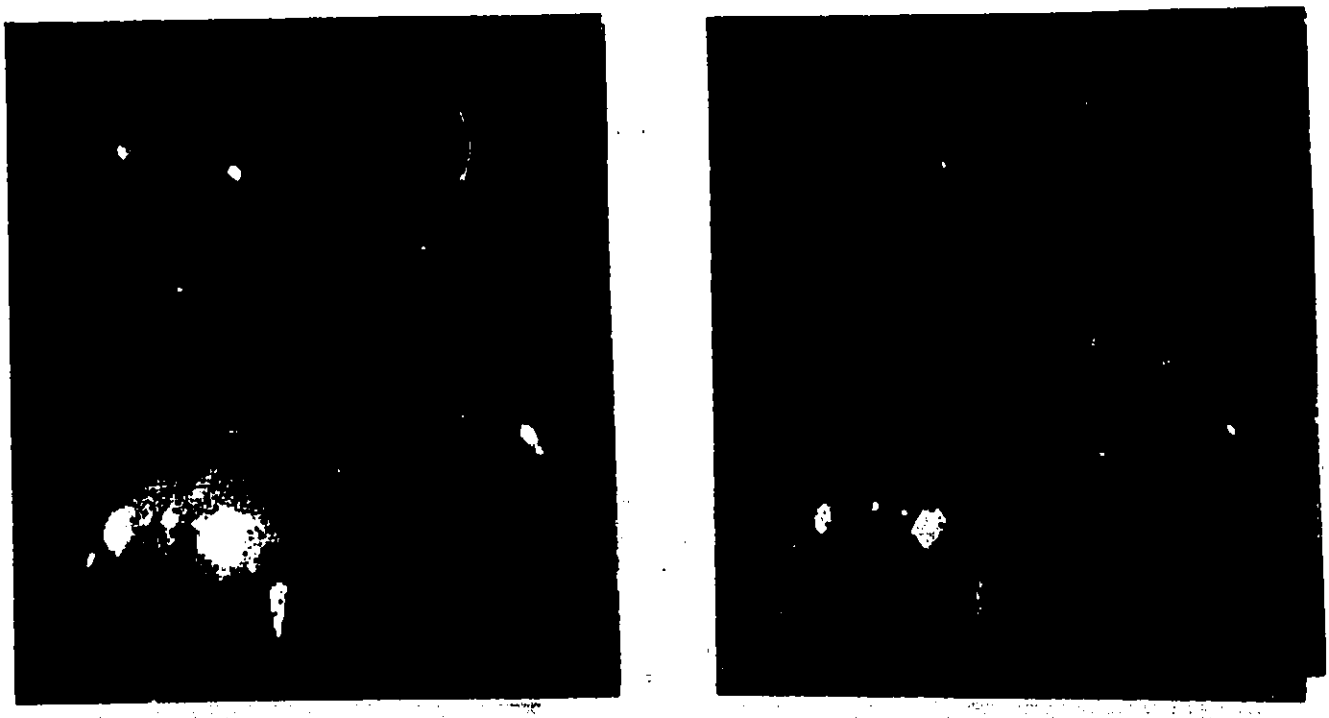

Figure 15a. RHEED images of the Si(100) surface in the <110> direction.

Figure 15b. RHEED images of the Si(100) surface in the <100> direction.

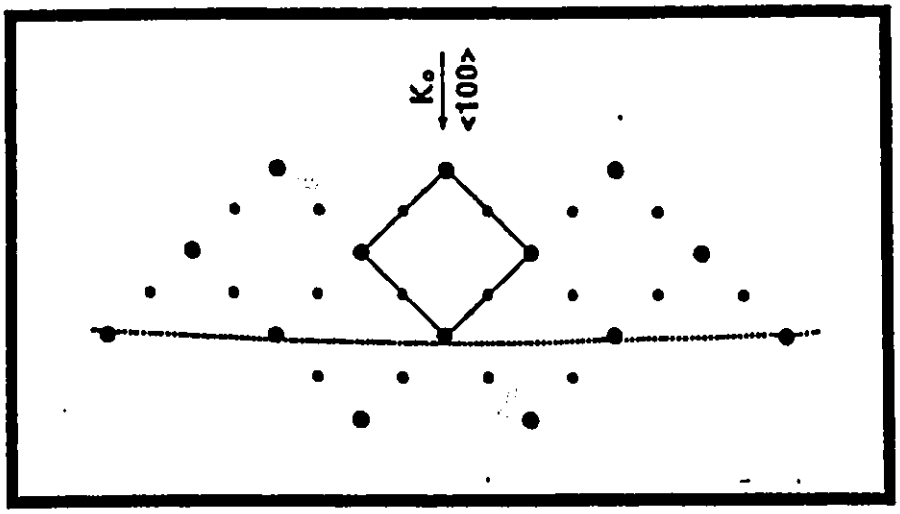

Figure 16. The reconstructed Si(100) surface diffraction pattern reveals a superposition of 2x1 unit cells.

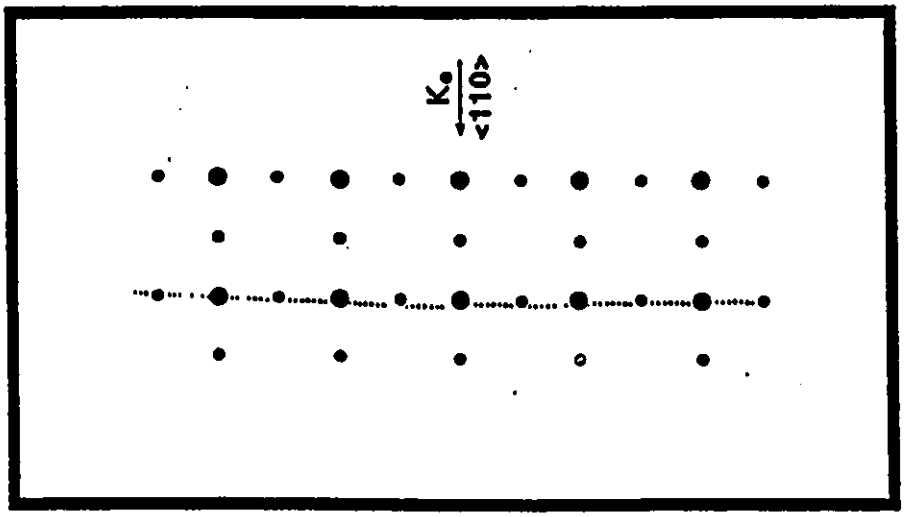

The sharpness of the spots of the RHEED pattern deteriorated with time. We attributed this to the adsorption of contaminants, mostly oxygen, at the surface. At our best pressures, $2x10^{-10}$ torr, a RHEED pattern in which the spots remained sharp was visible after leaving a clean sample overnight. At $5x10^{-9}$ torr, however, the spots lost their sharpness within 10 to 15 minutes indicating substantial surface coverage by foreign atoms.

The best test of surface cleanliness involved using ion-surface scattering, since the peaks present in a low energy ion scattering spectrum indicate the composition of the surface. For a positive incoming ion beam, only the scattered oxygen and recoiled silicon peaks appeared if the sample was properly cleaned. Additional peaks would indicate foreign atoms at the surface. As the sample became contaminated with the residual oxygen in the chamber the valley between the scattered and recoiled peaks was observed to fill in. In the middle of the 10^{-10} torr pressure range the ion scattering spectrum would show evidence of contamination within 45 minutes to an hour, whereas the RHEED pattern would show no visible signs of change. Fig.17a shows a spectrum from a target that was contaminated from residual oxygen. The valley between the recoiled Si and the scattered O^+ now has a large peak. An ozonated sample produced the spectrum shown in figure 17b. Neither the scattered oxygen nor the recoiled silicon can be identified. Only a peak produced by hydrogen adsorbed at the surface is observed.

The two distinct peaks corresponding to scattered oxygen and recoiled silicon are clearly seen in the energy spectrum of ions detected following collision with a sputtered and annealed target (fig18a). Below, a very similar energy spectrum using a target that had only been sputtered. The difference between the targets could be determined by looking at a RHEED image of each. The target that had been only sputtered would have an amorphous surface. The RHEED image of such an image would only show a uniform diffuse glow on the screen with neither diffraction spots nor Kikuchi lines present.

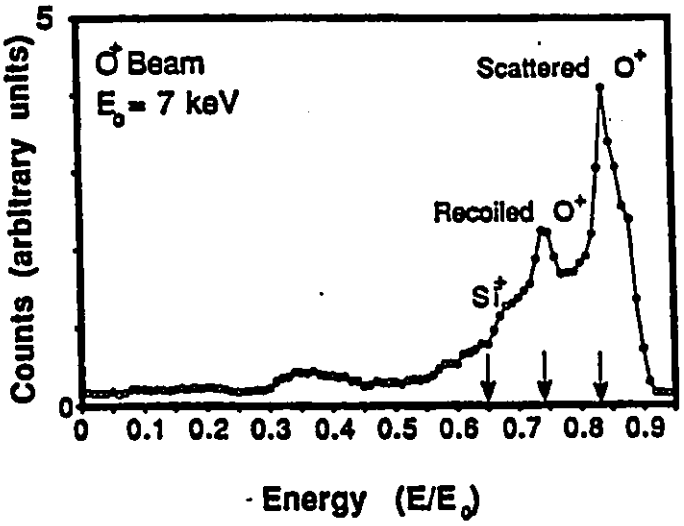

Figure 17a. LEIS spectrum of the Si(100) surface indicating sample contamination from residual gas.

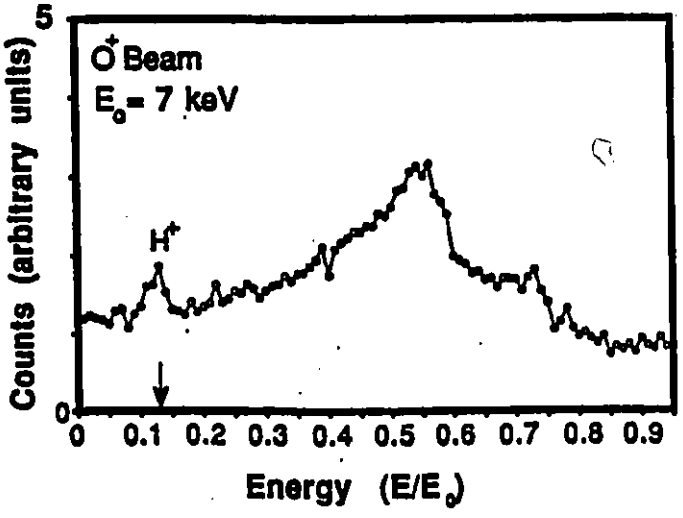

Figure 17b. LEIS spectrum of the ozonated Si(100) surface indicating extensive contamination.

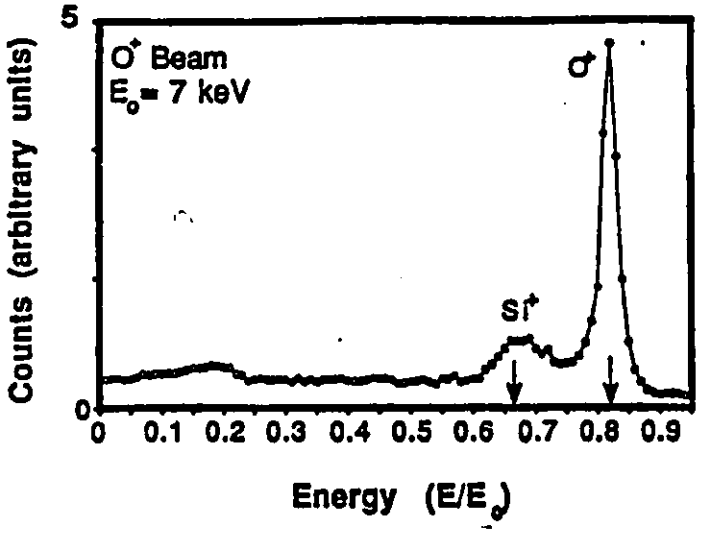

Figure 18a. LEIS spectrum of the Si(100) surface following sputtering and annealing.

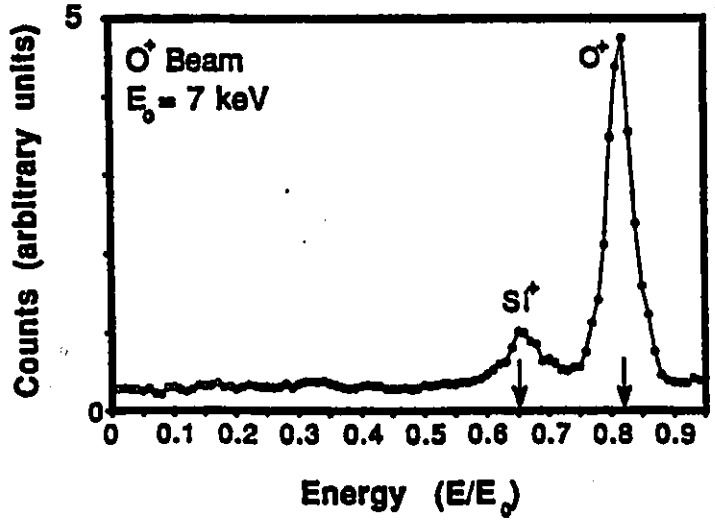

Figure 18b. LEIS spectrum of the Si(100) surface following sputtering only.

6.2 Hydrogen adsorption

Several attempts to reprcduce the hydrogen induced 1x1 structure were unsuccessful. In general, the following results were obtained. After a sputtered and annealed target had been left in an environment of Hydrogen at 10^{-6} torr for 10 minutes with the sputtergun filament and electron gun filament turned on, facing the target, the Hydrogen was pumped out of the chamber. The RHEED pattern resulting from this procedure showed a sharp 2x1 pattern identical to those obtained for clean samples, while ion-surface scattering spectra indicated that almost no hydrogen had adsorbed onto the surface. At the pressures used, 10 minutes should have been sufficient for a monolayer of hydrogen to adsorb onto the surface and hence alter the surface structure. Nonetheless, the procedure was repeated for longer times. The resulting RHEED patterns grew less sharp, indicating substantial coverage of the surface by foreign atoms. Ion-scattering spectra indicated substantial coverage of the surface by oxygen. We were confident that there were no leaks into the chamber. An analysis of the composition of the gas in the chamber using a mass spectrometer showed a very noticable presence of oxygen in the Hydrogen gas supply. Hence we concluded that a higher grade of Hydrogen must be obtained for this experiment. However, the likely explanation for our failure in preparing the dihydride surface was suggested by several experiments described in the literature which used a hot

filament in the vicinity of the surface of the sample to dissociate hydrogen atoms for adsorption at the surface[17].

6.3 Si(110)

6.3.1 The direction of cleavage of a Si(110) wafer

It was found that the edges of a cleaved sample of Si(110) met at an angle of approximately 70°. Possible cleavage directions can be selected from the four low index directions in the Si(110) plane, as shown in diagram 19, using the following formula to determine the angle between two directions:

$$\cos\phi = \frac{(l_1 l_2 + m_1 m_2 + n_1 n_2)}{\sqrt{l_1^2 + m_1^2 + n_1^2}\ \sqrt{l_2^2 + m_2^2 + n_2^2}}$$

where $[l_1, m_1, n_1]$ and $[l_2, m_2, n_2]$ are the two directions, and ϕ is the angle between them. Two possibilities exist which correspond to our observation. The angle formed between two <112> directions, i.e. [1$\underline{1}$2] and [$\underline{1}$12], is 70.5°. The same angle is formed between two <111> directions, i.e.[1$\underline{1}$1] and [11$\underline{1}$]. In order to positively identify the cleavage direction the angle between the surface and cleavage plane must be known.

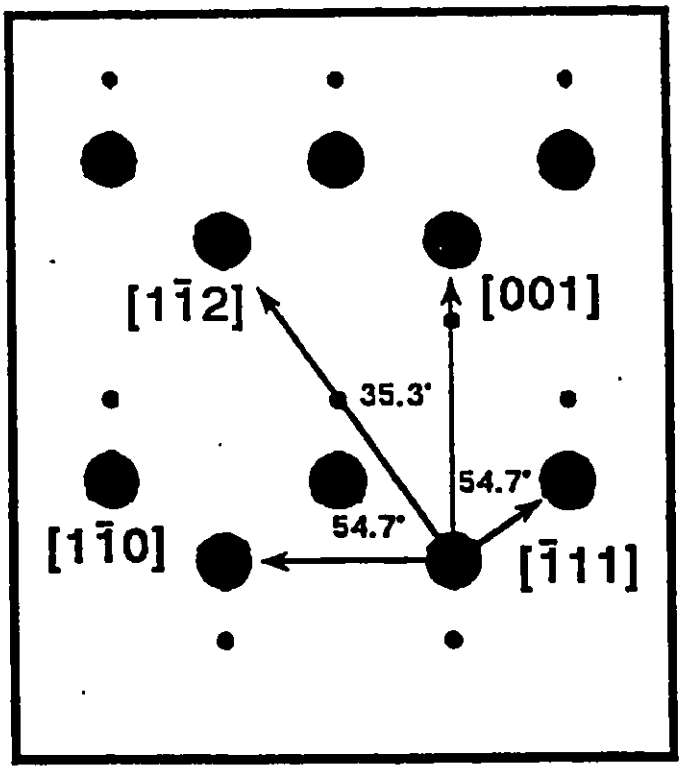

Figure 19. Major crystalographic directions in the Si(110) surface.

Observations of the cleavage edge of Si(110), using a microscope, showed that the edge is formed at 90° to the surface. It is well known that clean Si(111) and Si(110) surfaces can be obtained by cleaving[18], i.e. {111} and {110} are cleavage planes of the crystal. We can use the above formula to determine the angles at which these planes meet. The angle formed between the {110} and {$\underline{1}$11} directions is 90° while the angle between (110) and (100) is 60°. Thus we conclude that the wafer cleaves along {111} planes.

The cleavage direction is determined by the following formula:

$$u = \begin{vmatrix} m_1 & n_1 \\ m_2 & n_2 \end{vmatrix} , \quad v = \begin{vmatrix} n_1 & l_1 \\ n_2 & l_2 \end{vmatrix} , \quad w = \begin{vmatrix} l_1 & m_1 \\ l_2 & m_2 \end{vmatrix}$$

where [u,v,w] is the edge where the two planes (l_1, m_1, n_1) and (l_2, m_2, n_2) intersect. The (110) and ($\underline{1}$11) planes intersect along an edge running in the [1$\underline{1}$2] direction. This clearly identifies the cleavage direction as <112>, and the cleavage plane as (111).

6.3.2 Orientation

The cleaved sample was held by the manipulator clamps along a cleavage direction. With the manipulator set to 0° the electron beam would be incident at about a <112> direction. Let us say that the beam came in along the [$\bar{1}$12] direction.

A high symmetry RHEED pattern was observed at approximately 37.9° from the [$\bar{1}$12] direction. This corresponds closely to the 35.3° angle formed between the [$\bar{1}$12] and the [001] directions (see figure 20). A phase transition was observed as the sample cooled down. The specimen had been heated to 1050°C for 10 minutes followed by 750°C for 10 minutes. Directly following the heating many sharp spots were visible in the 0th Laue zone. After approximately 10 minutes, as the sample was cooling down, only half of these spots remained. This suggests that some kind of temperature dependent phase transition had occurred. As the sample temperature dropped over the following 20 minutes clear and distinct fractional Laue zones became stronger showing a clear 3-structure in the [001] direction. The temperature was not monitored during this time, however the 3-structure was stable for the duration of our observations. The whole order Laue zones consisted of alternating strong and weak spots which suggested a 2-structure.

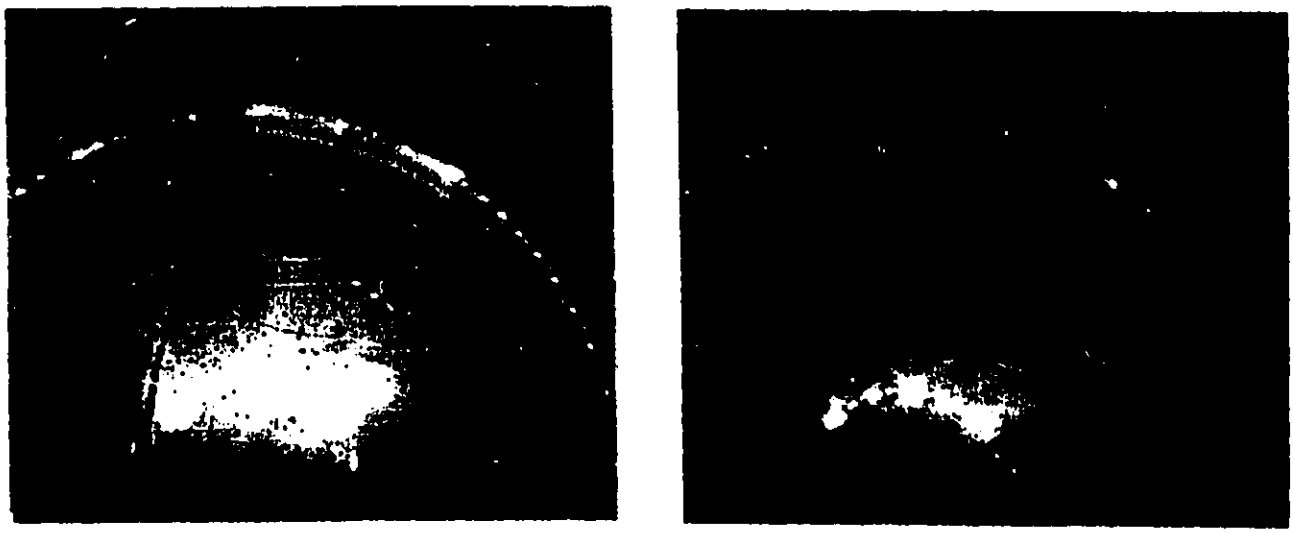

Figure 20. RHEED images of the Si(110) surface in the <100> direction.

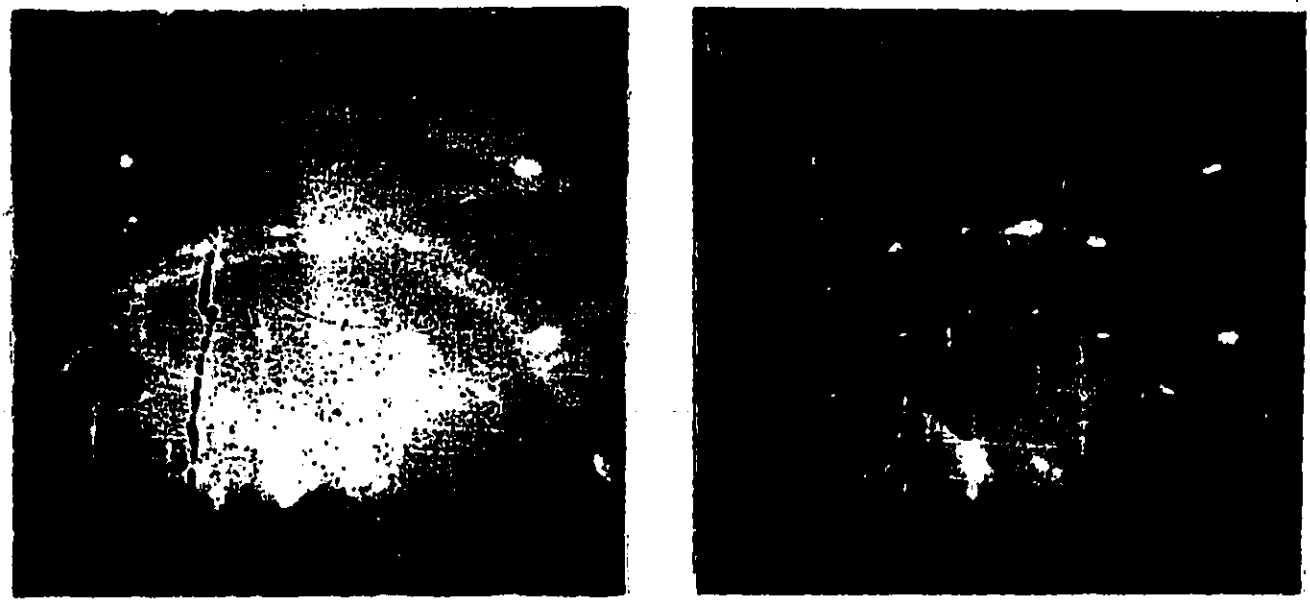

Figure 21. RHEED images of the Si(110) surface in the <111> direction.

At 15.5° on the other side of the [$\bar{1}$12] direction another high symmetry RHEED pattern was obtained. This corresponded to the [$\bar{1}$11] direction which should form an angle of 19.5°. Clear half order Laue zones were evident indicating a 2 x structure. Each Laue zone included equally spaced bright spots. Faint but distinct parallel lines cut the Laue zones, joining spots on different semicircles. Between each pair of lines that joined dots were seen two additional parallel lines. These two fractional lines between bright spots suggest a 3-structure.

Another high symmetry direction was obtained by turning the sample another 37.5°, for a total of 53° from [$\bar{1}$12]. The angle expected between [$\bar{1}$12] and [$\bar{1}$10] is 54.7°. The electron beam now traveled along the [$\bar{1}$10] direction and the pattern clearly shows a half order Laue zone suggesting a 2 x structure. No structures could be clearly identified between the bright spots on the Laue zones. The geometry of the sample holder was such that when rotated that far it cast a shadow over the 0th Laue zone. The 0th Laue zone always appears with the greatest intensity. The unavailability of information from the 0th Laue zone makes the observations along this symmetry direction inconclusive.

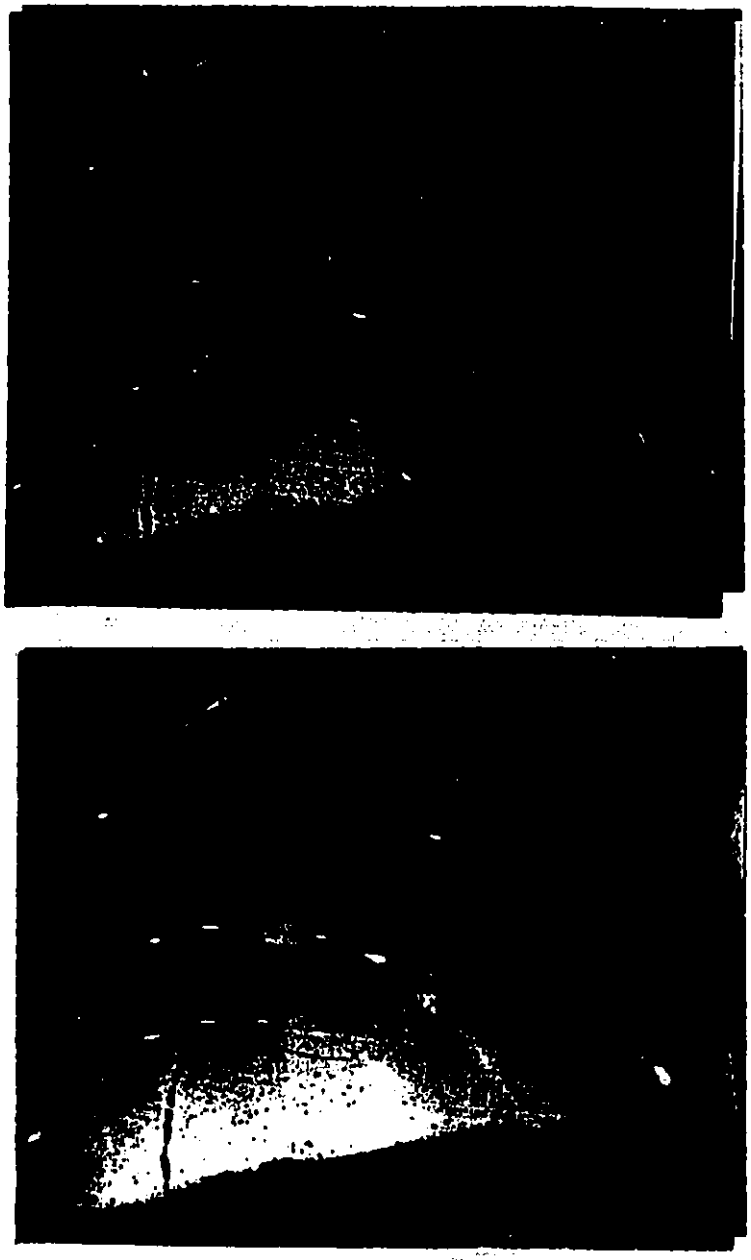

Figure 22. RHEED images of the Si(110) surface in the <110> direction.

The photographs of the RHEED patterns obtained for the other two symmetry directions seem to suggest some combination of 2 x and 3 x structure. A three structure, although it would fit the ((2n+1) x 1) phase for n=1 has never been reported. However this does not explain the 2 x periodicity which we observe. In addition, the ((2n+1) x 1) phases occur at high temperatures while the two fractional Laue zones for the [001] direction increased in intensity as the sample cooled down. It has been reported[19] that annealing at 700°C results in the facetting of the surface producing the complicated "X" pattern observed by many authors[20]. This may have occured in our experiment, however the current body of information we have obtained experimentally is not sufficient to make any conclusions.

It is evident that the RHEED image by itself does not provide sufficent information to explain the observed reconstructed image of the Si(110) surface. Firstly, we must be able to determine the extent of surface contamination and identify the foreign atoms at the surface. This will be possible using LEIS as described in the Si(100) section. Then a heating procedure will have to be developed which will result in a clean surface with the "16x2" structure. Van Loenan suggests that sample holders need to be annealed at 1000°C for several hours at UHV to get rid of any nickel or copper contaminants.

The discrepancy between the observed angles and those predicted by purely geometric considerations suggest that there is a considerable error associated with the azimuthal rotation control on the sample manipulator. Damage may have been caused from over-heating the manipulator assembly during baking of the UHV chamber.

Chapter 7. Conclusion

A fully operational system for the study of single crystal surfaces has been built. Included are facilities for in situ cleaning and annealing of the specimen. Pressures in the low 10^{-10} torr range are achieved routinely in the ultra-high-vacuum chamber, giving us ample time to carry out measurements.

The RHEED system which was constructed has been shown to provide reliable information about surface reconstruction and orientation. Its greatest value is that it provides an immediate indication of state of the surface. As a diagnostic tool it has been used extensively in the preparation of surfaces.

Although both positive and negative low energy oxygen ion beams can be produced, measurements concerned with the composition of crystal surfaces were taken using the stronger positive beam as it was easier to obtain and remained more stable over time. The energy spectra of scattered ions are a good indicator of the relative cleanliness of the surface.

Chapter 7. Conclusion

Preliminary investigations carried out on the Si(110) surface using RHEED indicate that the composition of the surface will have to be monitored using ion-surface scattering techniques if we hope to obtain the "16x2" pattern associated with a clean surface. Procedures developed using the Si(100) sample can be applied to the Si(110) surface. Preliminary experiments in which hydrogen is adsorbed onto clean Si(110) have recently been performed[21]. Our apparatus should be capable of performing similar studies.

APPENDIX1

The Ewald Sphere

Before discussing the Ewald sphere construction, a brief review of diffraction phenomena in general is in order [22]. In conventional diffraction experiments incident radiation is reflected by a sample which has regular periodicity. The periodicity should be of the same order of magnitude as the wavelength of the incoming radiation. Radiation of longer wavelength cannot resolve details of structure on an atomic scale. Silicon has a lattice parameter of 5.43Å, so that radiation of a few Å or less is required for a pattern in reciprocal space to be obtained. If the unit cell of a lattice is defined in terms of the unit vectors **a**, **b**, and **c**, then the reciprocal lattice is defined by the vectors **A**, **B**, and **C** satisfying the following relations

$$\mathbf{A} \cdot \mathbf{a} = \mathbf{B} \cdot \mathbf{b} = \mathbf{C} \cdot \mathbf{c} = 2\pi$$

and $$\mathbf{A} \cdot \mathbf{b} = \mathbf{B} \cdot \mathbf{c} = \mathbf{C} \cdot \mathbf{a} = \mathbf{A} \cdot \mathbf{c} = \cdots = 0$$

APPENDIX 1

The interpretation of this diffraction pattern is necessary in order to gain real space information about crystal structure.

Diffracted beams are produced when the reflections from parallel planes of atoms interfere constructively. Bragg's law states the condition for constructive reflection of the incident radiation

$$2d\sin\Theta=n\lambda$$

where d is the distance between reflection planes in the crystal, Θ is the angle the incident radiation makes with the plane of atoms, λ, the wavelenth of incident radiation and n is the order of reflection.

The Ewald sphere construction is useful as a visual representation of the diffraction condition when we discuss the characteristic features of RHEED patterns. It is illustrated by the figure on the next page. There is a vector representation of the diffraction condition which can be related to Bragg's law via the Ewald spere construction:

$$\underline{k}'-\underline{k}_o=\underline{g}$$

where $\underline{k}_o$ is the wavevector associated with incident radiation, $\underline{k}'$ is the reflected radiation wavevector, and $\underline{g}$ is the reciprocal lattice vector.

APPENDIX 1

If a reciprocal lattice point lies on the surface of the Ewald sphere, the condition for elastic scattering is satisfied and diffraction occurs. A vector $\underline{k}'$ from P to a point intersecting the Ewald sphere, corresponds to a diffracted beam. The vector $\underline{g}$ joins the tips of $\underline{k}_o$ and $\underline{k}'$, illustrating the vector condition for diffraction. From the diagram we see $2\underline{k}_o\sin\theta=\underline{g}$. Substituting $\underline{k}_o = 2\pi/\lambda$ and $\underline{g} = 2\pi/d$, we find $2d\sin\theta=\lambda$ which is Bragg's law.

APPENDIX 1

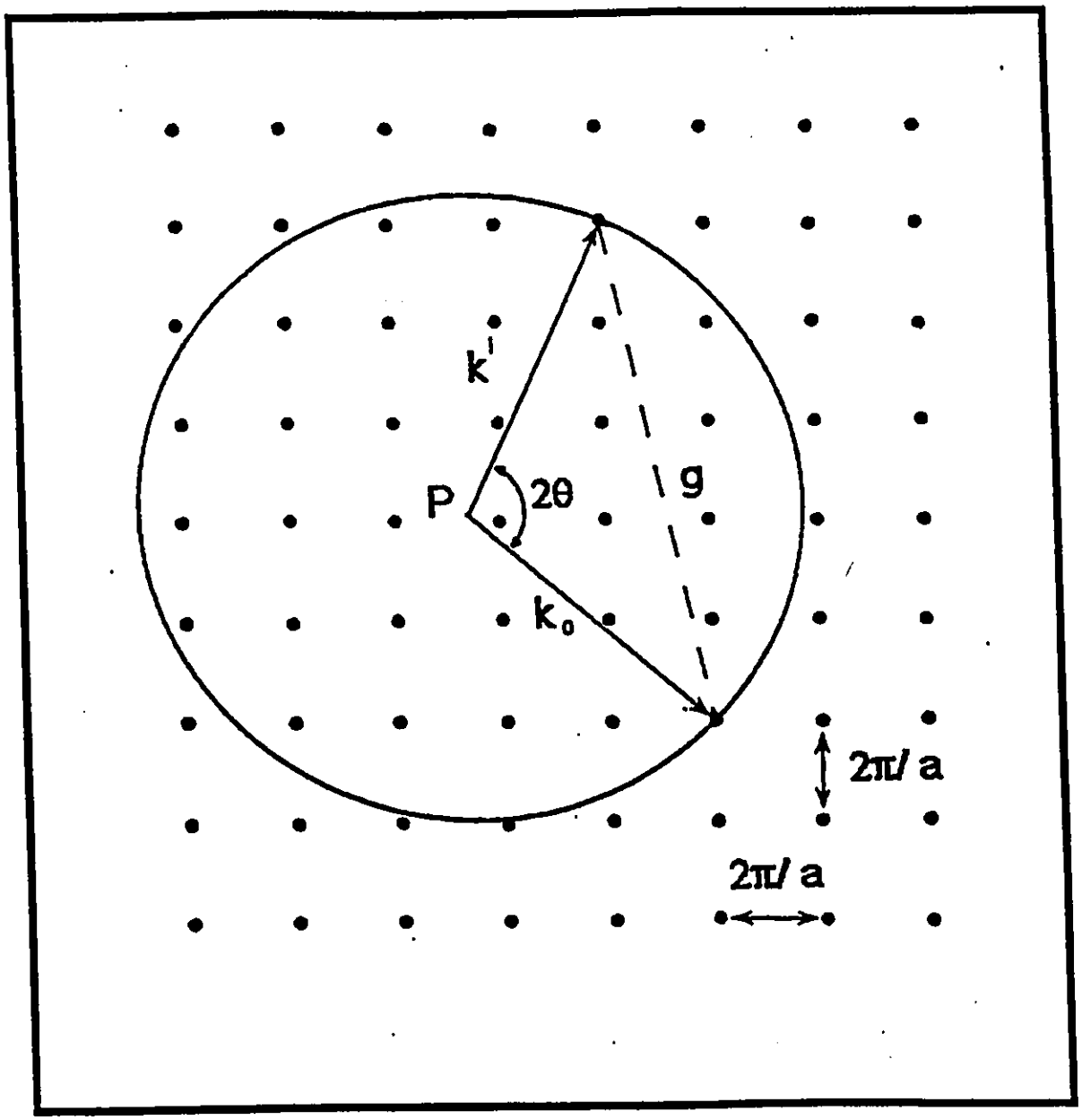

Figure 23. The Ewald sphere construction.

APPENDIX2

Notation

A simple notation to describe surface structures was devised by Wood[23]. It is best to give a few examples in order to get a feeling for it.

i) Si (100) (2x1)

Si refers to the bulk crystal. The surface normal in this case is (100). The surface to substrate mesh ratio is given by (2x1) indicating that the surface mesh is twice as large as the substrate mesh in one direction, with mesh edges parallel to those in the (100) plane.

ii) Si (100) c (4x2)

The letter c denotes a centred mesh. In this case the surface mesh is four times as large as the substrate mesh in one direction and twice as large in the other, with a point at the centre of the mesh.

iii) Si (100) p (2x2) ; Si (100) c (2x2)

The letter **p** denotes a primitive mesh, with equivalent points in the corners but none within the mesh. If there is only one structure with the given surface to substrate ratio the **p** can be omitted as was the case in example i) above. However in this case it is included in order to clearly discriminate between two different (2x2) structures.

iv) Si (100) (1x1) - H

The **H** at the end of the notation refers to an adsorbate at the surface, in this case hydrogen. The hydrogen causes the atoms at the surface to occupy bulk-like positions, indicated by (1x1).

v) Si (111) ($\sqrt{19}$x$\sqrt{19}$)R23.4° - Ni

When Ni is deposited onto the (111) surface of Si a structure forms at the surface which is rotated 23.4° to the underlying mesh. The points at the surface exhibit a long range periodicity that is $\sqrt{19}$ times that of the underlying bulk plane[24].

vi) Si (110) "16x2"

The structure at the clean Si(110) surface is highly complex and the standard notation is not sufficient to communicate all that needs to be stated in order to fully describe the structure. For instance, there is no notational form to represent the terraced structure that has been reported. Hence a short-hand notation is used to refer to the structure without attempting to provide a full description.

References

1. D. P. Smith, J. Appl. Phys. **38**, n.1, 340 (1967).

2. C. Davisson and L. H. Germer, Phys. Rev. **30**, 707 (1927).

3. P. J. Estrup and E. G. McRae, Surf. Sci. **25**, 1 (1971).

4. Electron Microscopy of Thin Crystals P. Hirsch, A. Howie, R. B. Nicholson, D. W. Pashley, and M. J. Whelan, Robert E. Krieger Publishing Company, Huntington, New York, 1977.

5. J. J. Lander and J. Morrison, J. Chem. Phys. **37**, 729 (1962).

6. M. Aono, Phys. Rev. Letters, **49** n.8, 567 (1982).

7. R. M. Tromp, Phys. Rev. Letters, **46**, n.14, 934 (1981).

8. D. J. Chadi, Appl. Optics, **19**, 3971 (1980); R. M. Tromp, R. G. Smeenk and F. W. Saris, Surf. Sci., **133**, 137 (1983)

9. F. Jona, IBM J. Res. Dev. **9**, 375 (1965).

10. B. Z. Olshanetsky and A. A. Shklyaev, Surf. Sci. **67**, 581 (1977).

11. T. Ichinokawa, H. Ampo, S. Miura and A. Takamura, Phys. Rev. B., **31**, 5183 (1985).

12. A. I. Shkrebtii, C. M. Bertoni, R. Del Sole and B. A. Nesterenko, Surf Sci **239**, 227 (1990).

13. E. J. van Loenen, D. Dijkkamp and A.J. Hoeven, Journal of Microscopy, **152**, Pt 2, 487 (1988).

14. T. Ichinokawa, H. Ampo, S. Miura and A. Tamura, Phys. Rev. B **31**, 5183 (1985).

15. L. C. Feldman, P. J. Silverman and I. Stengaard, Nucl. Instr. Meth. **168**, 589 (1980).

16. H. Ampo, S. Miura, K. Kato, Y. Ohkawa and A. Tamura, Phys. Rev. B **34**, n.4, 2329 (1986).

17. Ibid.

18. R. M. Feenstra, Joseph A. Stroscio and A. P. Fein, Surf. Sci. 181, 295 (1987); R. M. Feenstra and A. P. Fein, IBM J. Res. Develop., 30, n.5, 466 (1986).

19. P. Mårtensson, G. V. Hansson and P. Chiaradia, Phys. Rev. B 34, n.4, 2581 (1985).

20. B. Z. Olshanetsky and A. A. Shklyaev, Surf. Sci., 67, 581 (1977).

21. H. Ampo, S. Miura, K. Kato, Y. Ohkawa and A. Tamura, Phys. Rev. B 34, n.4, 2326 (1986).

22. Introduction to Solid State Physics, Third Edition, Charles Kittel, John Wiley & Sons, Inc., New York, London, Sydney, 1966.

23. Elisabeth A. Wood, J. Appl. Phys. 35 n.4, 1306 (1964).

24. R. J. Wilson and S. Chiang, Phys. Rev. Lett. 58, 2575 (1987).